J. Electrochem. Sci. Eng. **15(2)** (2025) 2544; https://doi.org/10.5599/jese.2544

Open Access : : ISSN 1847-9286
www.jESE-online.org

Original scientific paper

Evaluation of porphyrin molecules as effective corrosion inhibitors for copper alloy in sulfuric acid using both experimental and computational approaches

Metwally Abdallah[1,2,✉] , Majda Alfakeer[3,✉] , Rasha N. Felaly[1], Abdulaziz M. Almohyawi[1], Jabir H. Al-Fahemi[1], Salih S. Al-Juaid[4], Doaa F. Seyam[2], Elsayed M. Mabrouk[2] and Kamal A. Soliman[2]

[1]*Chemistry Department, Faculty of Sciences, Umm Al-Qura University, Makkah, Saudi Arabia*
[2]*Chemistry Department, Faculty of Science, Benha University, Benha, Egypt*
[3]*Chemistry Department, Faculty of Science, Princess Nourah bint Abdulrahman University, Riyadh, Saudi Arabia*
[4]*Chemistry Department, Faculty of Science, King Abdulaziz University, Jeddah, Saudi Arabia*

Corresponding author: ✉metwally555@yahoo.com; ✉msalonazi@pnu.edu.sa

Received: October 24, 2024; Accepted: January 6, 2025; Published: February 3, 2025

Abstract

The inhibition efficacies of two porphyrin molecules, namely, 5,10,15,20-tetra-[m-(methoxy) phenyl] porphyrin (m-TMPP) and 5,10,15,20-tetra-[p-(methoxy)phenyl] porphyrin (p-TMPP) on the corrosion of copper alloy (C12510) in 1.0 M H_2SO_4 solutions were examined. Some chemical, electrochemical measurements, density functional theory and Monte Carlo simulations were utilized to study the adsorption behaviour and corrosion inhibition efficiency of m-TMPP and p-TMPP on the Cu (111) surface in acidic media. Scanning electron microscopy analysis was employed to examine the surface morphologies of the tested C12510 surfaces. The outcomes of these techniques proved that the inhibition efficiency increases with increasing concentration of TMPP molecules and with lowering temperatures. The inhibition efficiency is reached to 96.23 and 97.61 % in the case of m-TMPP and p-TMPP, respectively, using the potentiodynamic polarization technique. The inhibitory effect of TMPP molecules is explained based on their spontaneous physicochemical adsorption on the surface of C12510. The adsorption process is obeyed by the Langmuir isotherm model. Additionally, some thermodynamic activation parameters were determined and discussed. It was discovered that the two TMPP compounds retarded the pitting corrosion of C12510 in chloride-containing solutions by shifting the pitting potential to a more noble direction. Based on all the approaches investigated, the inhibitory efficacy of p-TMPP is higher than that of m-TMPP at every concentration tested.

Keywords
Metal alloy corrosion; heterocyclic organic compounds; adsorption isotherm; pitting potential; surface morphology; quantum chemical calculations

Introduction

Copper is a vital element used in many strategic industries due to its numerous qualities, including its low price, electrical conductivity, and distinctive mechanical properties. It is mainly used in electrical appliances, chemical industries, printed circuit boards, copper strips for shielding wires, airbags, busbar terminals, electromagnetic switches, pen holders, and roof panels [1]. Copper is a corrosion-resistant metal. Usually, 1.0 M H_2SO_4 solution is applied in pickling, cleaning processes, and removing precipitation layers on the copper surface, but, unfortunately, corrosion of the copper occurs, causing many economic problems. Researchers have tried a variety of approaches to eliminate or slow down copper corrosion, the most significant of which is the utilization of corrosion inhibitors because of their simple operation and remarkable effects [2].

Many of the inhibitors used for copper corrosion in acidic solutions are organic molecules with heteroatoms; the most common ones are nitrogen, oxygen, phosphorus, and sulphur; they are employed as inhibitors for copper corrosion in acidic solutions. These organic compounds' ability to prevent corrosion is dependent upon the heteroatoms they contain and typically decreases in the following order: P > S > N > O [3]. Numerous compounds, including drugs, synthetic organic molecules, and plant extracts, have been demonstrated to have effective inhibition efficiency against copper corrosion [4-6]. The efficiency of an inhibitor was influenced by the environment it operated in, the metal surface characteristics, and the interface electrochemical potential [7]. It is widely recognized that the initial stage in the mechanism of inhibition of copper in sulfuric acid solution is the adsorption of the organic molecules onto its surface. The main factors determining the force of adsorption operation are the chemical structure of the adsorbed compound, its properties like electron density (orbitals that donate electrons), aromaticity, and functional groups [8]. Also, density functional theory (DFT) calculations allow the prediction of molecular properties, which are key indicators of the ability of a molecule to donate or accept electrons. These electronic descriptors are essential for understanding how well an inhibitor can interact with a metal surface. Porphyrin derivatives have previously been used as corrosion inhibitors for 304 stainless steel in acidic environments [9] and N80 steel in 3.5 % sodium chloride solution [10]. The inhibitory effect of these compounds is due to strong adsorption on the steel surface.

The main objective of this manuscript is to determine the success of novel synthetic porphyrin molecules in suppressing the corrosion of copper alloy (C12510) in 1.0 M sulfuric acid solution using chemical and electrochemical methods. Scanning electron microscopy (SEM) was used to analyze the surface morphology of the copper sample. We supported our results by confirming the experimental results with calculated quantitative chemical parameters obtained from DFT and Monte Carlo (MC) simulations. Additionally, this study attempts to explicate the adsorption of porphyrin molecules on copper surfaces and understand the role of porphyrin structure in the corrosion inhibition process.

Experimental

Materials

The composition of the copper alloy (C12510) applied in this study is as follows**:** Cu (99.9 wt.%), Pb (0.020 wt.%), Zn (0.080 wt.%), Fe (0.05 wt.%), P (0.03 wt.%), Sb (0.003 wt.%), Te (0.025 wt.%), Sn (0.05 wt.%), Ni (0.050 wt.%) and Bi (0.005 wt.%). All chemicals used in this study were analytical grade (Aldrich chemicals). Distilled water was used to prepare corrosive solutions. 1.0 M H_2SO_4 was prepared using H_2SO_4 (98 %). The desired temperature of each experiment was adjusted to ±1 °C using an air thermostat.

Synthesis of inhibitors

Solvents and reagents were purchased from commercial suppliers and were applied without further purifying. A Buchi rotary evaporator was used to evaporate the solvent at a lower pressure.

^{1}H NMR and ^{13}C NMR spectra were gathered at 600 MHz on a Bruker Avance III™ HD 600 MHz spectrometer in 5 mm diameter tubes. Signals are presented in δ / ppm, from δ = 0.00 ppm (tetramethylsilane). All was done with deuterated chloroform solvent at room temperature. Ultraviolet-visible absorption spectra were recorded on Shimadzu® UV-1800 Spectrophotometer in solvent as stated. IR spectra were recorded using a Shimadzu® IRSpirit Fourier transform infrared spectrophotometer.

Thin layer chromatography (TLC) was employed using TLC plastic sheets coated with Silica Gel 60 F_{254} (MERCK®), and the compounds were visualized under short-wavelength UV light at 245 or 366 nm.

Scheme 1 presents the synthesis of 5,10,15,20-tetra-[p-(methoxy)phenyl] porphyrin (p-TMPP).

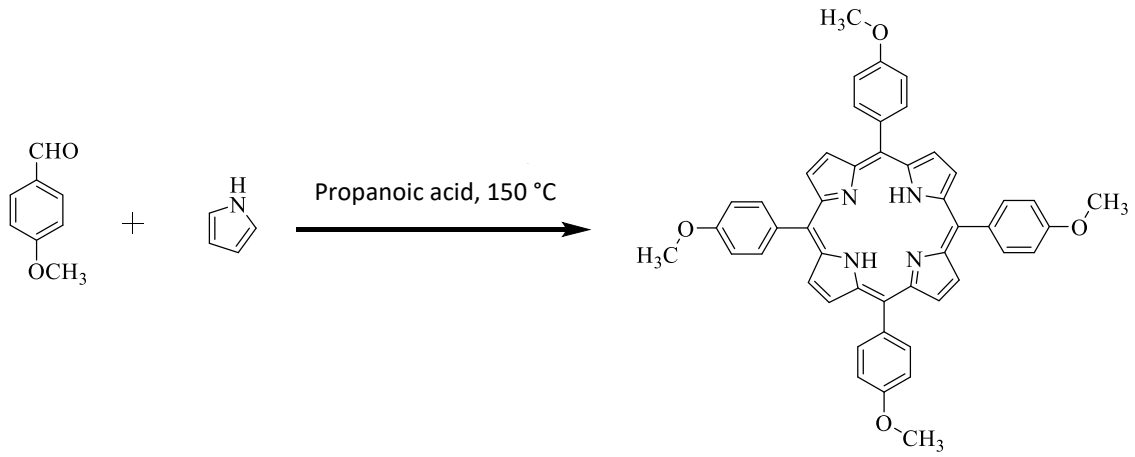

Scheme 1. *Synthesis of p-TMPP*

P-methoxybenzaldehyde (6.80 g, 50 mmol, 1 eq.) was added dropwise to newly distilled pyrrole (3.35 g, 50 mmol, 1 eq.) in refluxing propionic acid (100 ml) in a modified version of Adler's general procedure [11]. After allowing the mixture to cool to room temperature and refluxing it for 30 min at 150 °C, 150 ml of MeOH was added. The mixture was refrigerated for a week before being filtered and given another methanol cleaning. A recrystallization from chloroform/methanol afforded purple solid of title compound (1.82 g, 20 %); mp. >350 °C; Rf = 0.8 (Chloroform/Hexane; 1:1); ^{1}H NMR (600 MHz, $CDCl_3$) δ = 8.87 nm (s, 8H), 8.13 (d, J = 8.5 Hz, 8H), 7.29 (d, J = 8.5 Hz, 8H), 4.10 (s, 12H), -2.75 (s, 2H). ^{13}C NMR (151 MHz, $CDCl_3$) δ = 55.6, 112.2, 112.2, 119.7, 134.7, 135.6, 159.4 nm.

Scheme 2 presents the synthesis of 5,10,15,20-tetra-[m-(methoxy)phenyl] porphyrin (p-TMPP).

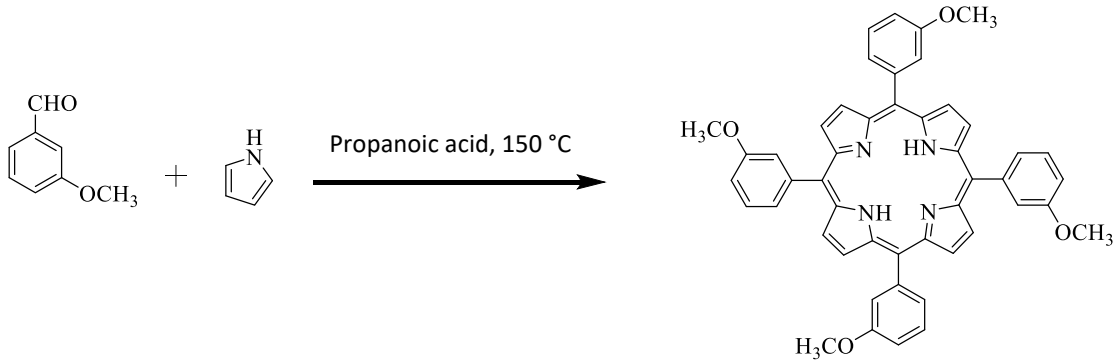

Scheme 2. *Synthesis of m-TMPP*

Freshly distilled pyrrole (3.35 g, 50 mmol, 1 eq.) was added dropwise to m-methoxybenzaldehyde (6.80 g, 50 mmol, 1 eq.) in refluxing propionic acid (100 ml) in accordance with a modified version of Adler's general approach [12]. The mixture was refluxed for 30 minutes at 150 °C. Once it had cooled to room temperature, 150 ml of methanol was added. After a week of refrigeration, the mixture was filtered and again cleaned with methanol.

A recrystallization from chloroform/methanol afforded purple solid of title compound (1.82 g, 20 %); mp.>350 °C; Rf=0.85 (Chloroform/Hexane; 1:1); ^{1}H NMR (600 MHz, $CDCl_3$) δ = 8.90 nm (s, 8H), 7.83 (d, J = 7.3 Hz, 4H), 7.80 (s, 4H), 7.65 (t, J = 7.9 Hz, 4H), 7.35 (dd, J = 8.4, 2.6 Hz, 4H), 3.99 (s, 12H), -2.78 (s, 2H). ^{13}C NMR (151 MHz, $CDCl_3$) δ = 55.5, 113.6, 119.9, 120.5, 127.5, 143.5 nm.

Weight loss technique

Thirteen coupons of C12510 were cut equally into (2.5×1.5×1) cm^3 cuboids and then polished with a series of emery papers (grades 320, 600, 800 and 1200) and then washed with bi-distilled water, acetone and distilled water before being air-dried. The C12510 samples were immersed in a blank solution of 1.0 M H_2SO_4 solution and solutions containing different concentrations of m-TMPP and p-TMPP. They were raised from their respective solutions after 2 hours, wiped with filter paper to remove the corrosion products and then weighed, all carefully done at approximately the same time. This process was repeated for different immersion periods (4, 6, 8, 10, 20 and 24 hours), at 298 K. WL technique was also performed for 1 M blank H_2SO_4 solution, 1.0 M H_2SO_4 solution containing 1 mM m-TMPP and 1.0 M H_2SO_4 solution containing 1 mM p-TMPP at temperatures of 313, 323, 333 and 343K. WL experiments were performed twice, and the average weight loss was calculated. The corresponding corrosion rate (CR_W / mg cm^{-2} h^{-1}) and the inhibition efficiency (η) were estimated by Equations (1) and (2) [13]:

$$CR_W = DW / At \quad (1)$$

$$\eta_W = \frac{CR_{un} - CR_{in}}{CR_{un}} 100 \quad (2)$$

where, t / h is the immersion time, A / cm^2 is the exposed area of the copper samples, ΔW / mg is the weight difference (before and after immersion) for the estimated time, and CR_{un} and CR_{in} represent the corrosion rate in uninhibited and inhibited solution, respectively.

Electrochemical techniques

Potentiodynamic polarization (PP) and potentiodynamic anodic polarization (PAP) techniques were conducted employing a PGSTAT30 potentiostat/galvanostat with a three-electrode cell; a calomel electrode (SCE), a counter platinum electrode (Pt) and the copper alloy (C12510) working electrode, with the exposed surface area of 0.25 cm^2. After the electrode was submerged in the test solution for around 60 minutes, or until the steady state potential was attained, the polarization process was initiated. For the PP and PAP techniques, the scan rates were set at 2.0 and 0.1 mV s^{-1}, respectively. In a temperature-controlled system, all procedures were done at 303 K. The electrochemical impedance spectroscopy (EIS) technique was conducted at open circuit potential (OCP) *via* peak-to-peak AC signal, with an amplitude of 4.0 mV and frequency range of 100 kHz to 0.1 Hz. Before being used, the exposed portion of the C12510 electrode was polished, cleaned for five minutes with distilled water and acetone, and then dried. At room temperature (25 °C), the corrosion data were recorded once as the potential reached the steady state values. The quantitative parameters of the dissolving properties were computed after analyzing the Nyquist and Bode plots.

The inhibition efficiency (η) obtained from PP and EIS was determined by the Eqs. (3) and (4) [14]:

$$\eta_{PP} = \left(\frac{i_{un} - i_{in}}{i_{un}} \right) 100 \quad (3)$$

$$\eta_{EIS} = \left(\frac{R_{ct,in} - R_{ct,un}}{R_{ct,in}} \right) 100 \quad (4)$$

where, i_{un} and i_{in}, are corrosion current densities for uninhibited and inhibited solutions correspondingly, while $R_{ct,un}$ and $R_{ct,in}$ are the resistance of charge transfer for uninhibited and inhibited solutions, respectively.

Scanning electron microscopy analysis

SEM analysis for specimens was done in 100 ml of blank 1.0 M H_2SO_4 solution and with 1.0 mM of m-TMPP and p-TMPP for 2 h. Then specimens were taken off, washed with acetone, and then dried. The analysis was done using a JSM-IT700HR/LA SEM, at a 15 kV acceleration voltage.

Density functional theory study

Density functional theory (DFT) is a frequently utilized instrument in corrosion research because of its ability to accurately model and predict the molecular properties of many substances. In this study, the molecular structures were drawn using GaussView software [15], while the Gaussian 09 suite was used for performing DFT calculations [16]. Specifically, the B3LYP functional with the 6-31G(d,p) basis set was employed to optimize the geometries of the m-TMPP and p-TMPP molecules [17]. To better represent the surrounding environment, calculations were performed for an aqueous phase using the conductor-like polarizable continuum model [18]. Using DFT**,** frontier molecular orbital (FMO) properties were calculated. These provide insights into the molecule's reactivity, as HOMO represents the molecule's electron-donating ability, and LUMO corresponds to its electron-accepting ability. Other key electronic descriptors derived from the FMO analysis include global hardness (γ)**,** global softness (σ)**,** and Fraction of transferred electrons (ΔN_{111}) that are calculated according to Equations (5) to (7):

$$\gamma = \frac{E_{LUMO} - E_{HOMO}}{2}. \quad (5)$$

$$\sigma = \frac{1}{\gamma} \quad (6)$$

$$\Delta N_{111} = \frac{\varphi - \chi_{inh}}{2(\gamma_{Cu} + \gamma_{inh})} \quad (7)$$

where φ is the work function of Cu surface (4.94 eV), and χ is the electronegativity of inhibitor.

Monte Carlo simulation

To explore the interaction between m-TMPP and p-TMPP with the Cu (111) surface, we employed a Monte Carlo (MC) simulation approach to model the adsorption process at the atomic scale. The interaction energies and adsorption configurations were calculated using the Adsorption Locator module in Materials Studio 2017 software [19]. The Cu (111) surface was chosen for its stability and relevance in corrosion studies. We modelled a supercell of the copper surface using periodic boundary conditions to simulate an extended surface area. A slab model of the Cu (111) surface was generated, with a 3.0 nm vacuum in the *z*-direction above the surface. This setup represents a large enough surface area to explore multiple adsorption sites for the molecules and solvent interactions. The copper surface was constructed with 9×9 unit cells, resulting in a supercell with sufficient space to accommodate the inhibitors and solvent molecules. To simulate an acidic environment, which is crucial for studying the corrosion process, we

introduced 100 water molecules as the solvent, four hydronium ions (H_3O^+) and two sulphate ions (SO_4^{2-}) were incorporated into the simulation box. The entire simulation system (Cu surface, water molecules, hydronium ions, sulphate ions, and inhibitors) was optimized using the Forcite module in Materials Studio. The COMPASS force field was applied for all components of the simulation [20]. The COMPASS force field is well-suited for organic and inorganic systems and has been validated for surface interactions, making it ideal for simulating the interaction of inhibitors with metal surfaces. Energy minimization was applied to find the most stable configuration of the system, ensuring that all components are at their lowest possible energy states.

Results and discussion

Open circuit potential measurement

The open circuit potential (OCP) was measured over one hour while the copper working electrode was immersed in a 1.0 M H_2SO_4 solution. Figure 1 shows that the OCP values stabilize after about ten minutes. Moreover, the investigated TMPP compounds considerably diminish the cathodic corrosion process, as the OCP values become more negative than the blank.

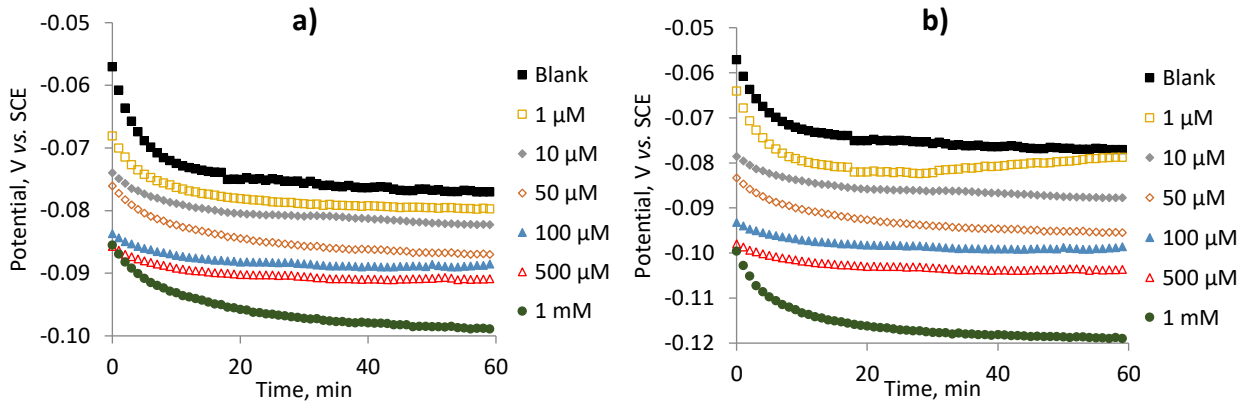

Figure 1. *Open circuit potential of C12510 alloy versus time in 1.0 M H_2SO_4 solution without and with different concentrations of a) m-TMPP and b) p-TMPP*

Potentiodynamic polarization technique

Figure 2 presents the PP curves of the C12510 electrode in blank 1.0 M H_2SO_4 and with different m-TMPP and p-TMPP molecule concentrations that vary from 10 µM to 10 mM. The estimated parameters from the anodic and cathodic curves, such as Tafel slopes, anodic (β_a) and cathodic (β_c), corrosion potential (E_{corr}), corrosion current density (i_{corr}) and inhibition efficiency (η_{pp}), are listed in Table 1.

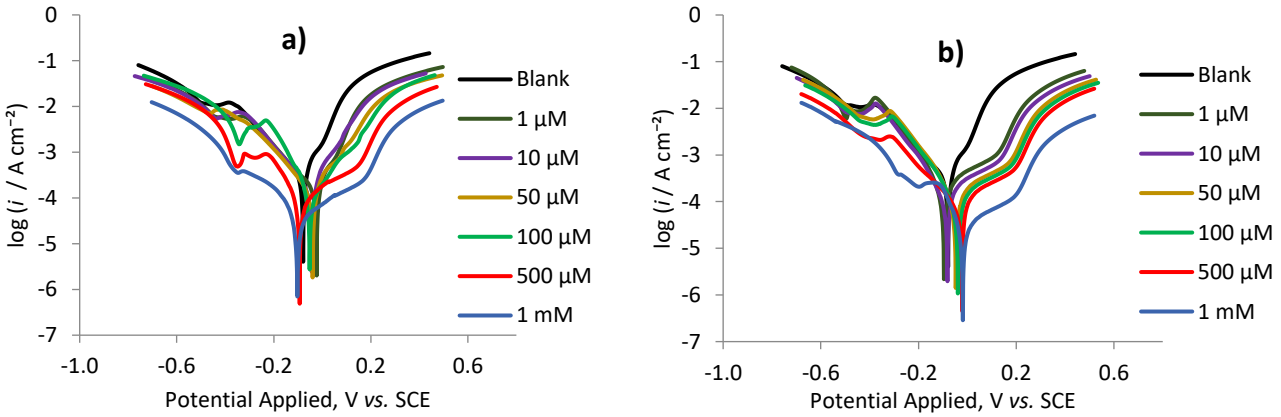

Figure 2. *PP curves for C12510 alloy in 1.0 M H_2SO_4 solution without and with different concentrations of a) m-TMPP and b) p-TMPP, at scan rate 2.0 mV s^{-1} at 298 K*

Table 1. *Electrochemical corrosion parameters of C12510 alloy in 1.0 M H_2SO_4 solution and with different TMPP doses at scan rate 2* mV s^{-1} *and 298 K*

	C / μM (at 298 K)	$-\beta_c$ / mV dec^{-1}	β_a / mV dec^{-1}	$-E_{corr}$ / mV	i_{corr} / μA cm^{-2}	CR_{PP} / mm $year^{-1}$	η_{PP}
Blank		48	62	79	2630.0	30.9	-
m-TMPP	1	49	63	23	1321.3	15.5	49.76
	10	50	65	44	864.4	10.2	67.13
	50	48	68	40	839.2	9.9	68.09
	100	45	70	52	680.5	8.0	74.13
	500	42	71	93	198.2	2.3	92.46
	1000	40	72	103	99.1	1.2	96.23
p-TMPP	1	34	58	96	844.0	9.9	67.91
	10	34	60	81	727.3	8.6	72.35
	50	35	62	48	479.3	5.6	81.78
	100	35	63	39	468.8	5.5	82.17
	500	35	64	20	196.1	2.3	92.54
	1000	36	65	18	62.9	0.7	97.61

The PP curves in 1.0 M H_2SO_4 in the absence and the presence of different concentrations of TMPP compounds shift to lesser current densities without a significant change in the shapes and slopes of the curves upon increasing the TMPP concentrations. This finding confirms the TMPP inhibitory ability of C12510 alloy against acid corrosion, by reducing the corrosion reaction rate without changing its mechanism. Anodic and cathodic current densities are significantly reduced with increasing m-TMPP and p-TMPP concentrations. This implies that the adsorption of porphyrin molecules, which probably blocks the active sites on the C12510 surface within the corrosive electrolyte, efficiently suppresses the dissolution of anodic metal and the development of cathodic hydrogen. The values of i_{corr} are reduced upon the increase of the TMPP concentrations and the η_{PP} increases, proving the inhibitory impact of these compounds.

The values of Tafel slopes (β_a and β_c) were nearly unchanged in the presence of porphyrin molecules. The change in β_a is about 10 and 3 mV dec^{-1} in the case of m-TMPP and p-TMPP, respectively, while the change in β_c is about 8 and 12 mV dec^{-1} in the case of m-TMPP and p-TMPP. Also, the E_{corr} values change within less than ±85 mV away from the blank by increasing TMPP concentration. This implies that porphyrin compounds operate as mixed-type inhibitors *via* inhibiting both anodic and cathodic corrosion reactions [21].

A drop of the current density in the cathodic region is observed, followed by an irreversible increase as the potential decreases. Also, a potential plateau is seen where the Cu electrode crosses the Tafel polarization zone in the anodic region. In this region, the current value barely changes with the potential increase before its irreversible increase as the potential increases further. This phenomenon is probably due to the formation of the porous surface layer of corrosion products.

Potentiodynamic anodic polarization

PAP curves for a C12510 electrode in blank 1.0 M H_2SO_4 and with different quantities of NaCl added as a pitting corrosion factor at a scan rate of 0.1 mV s^{-1} are displayed in Figure 3. The slow scan rate reduces the chance for pitting at a lower potential [22]. The lack of a dissolving peak confirms the stability of the coating layer grown on the surface of C12510. Until a certain potential is achieved, the current increases rapidly due to the passive layer built on the surface of C12510 and the pitting corrosion progresses. This potential is known as the pitting potential ($E_{pitt.}$).The reduction of passivity can originate from the adsorption of Cl^- ions on the passive film that develops on the C12510 surface, which generates an electrostatic field through the film/electrolyte interface [23]. Thus, at a certain magnitude of the electrostatic field, the adsorbed anions start to enter the passive film and the pitting corrosion develops.

Assessment of the electrode surface after PAP tests showed visible pits, the number of which increased with increasing chloride ion content in the solution.

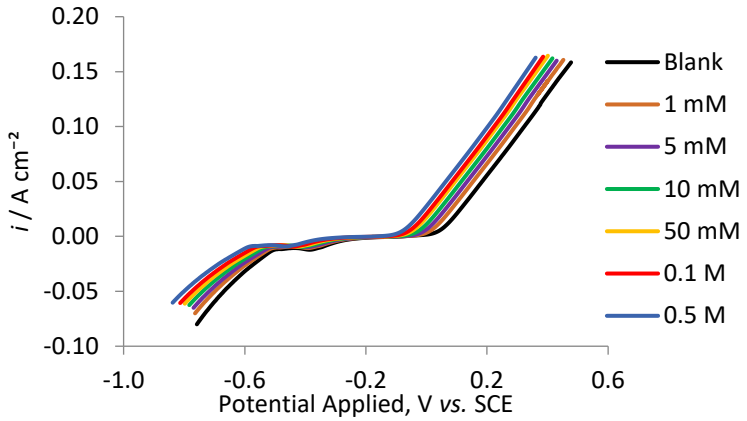

Figure 3. *Potentiodynamic anodic polarization curves for C12510 alloy in 1.0 M H_2SO_4 solution and different concentrations of NaCl at room temperature, at scan rate 0.1 mV s^{-1} and 298 K*

The correlation between E_{pitt} and log Cl^- is described in Figure 4. A straight-line relationship that fulfils the equation below [24]:

$$E_{pitt} = \alpha - \beta \log C_{Cl^-} \quad (8)$$

where α and β rely on the concentration of aggressive ions, as well as the type of metal or alloy. When the concentration of Cl^- ion increases, E_{pitt} values are moved to the active negative direction, proving that the Cl^- ion speeds the formation of pitting corrosion. TMPP molecules were tested as inhibitors for pitting corrosion utilizing the PAP technique.

The PAP curves for the C12510 electrode in a solution of 1.0 M H_2SO_4 + 0.5 M NaCl without and with certain concentrations of m-TMPP and p-TMPP molecules, respectively, are represented in Figure 5 at a scan rate of 0.1 mV s^{-1}.

It has been discovered that the E_{pitt} of the C12510 electrode is moved to more noble values with increasing the concentration of TMPP molecules. This implies increased protection of the C12510 electrode from pitting attack.

The relation between the logarithmic of the molar concentration of the TMPP molecules and E_{pitt} is displayed in Figure 6. Straight lines are acquired by satisfying Equation (9):

$$E_{pitt} = a - b \log C_{TMPP} \quad (9)$$

where a and *b* rely on the inhibitor employed as well as the type of metal or alloy.

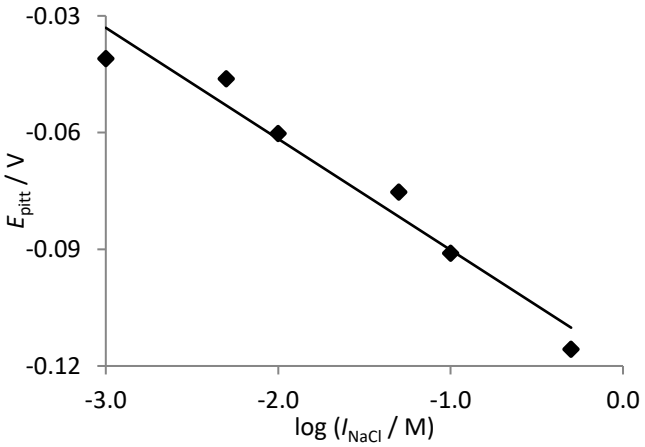

Figure 4. E_{pitt} vs. *log* C_{Cl^-} *ions for C12510 alloy in 1.0 M H_2SO_4 solution with various concentrations of NaCl, at scan rate 0.1 mV s^{-1} and 298 K*

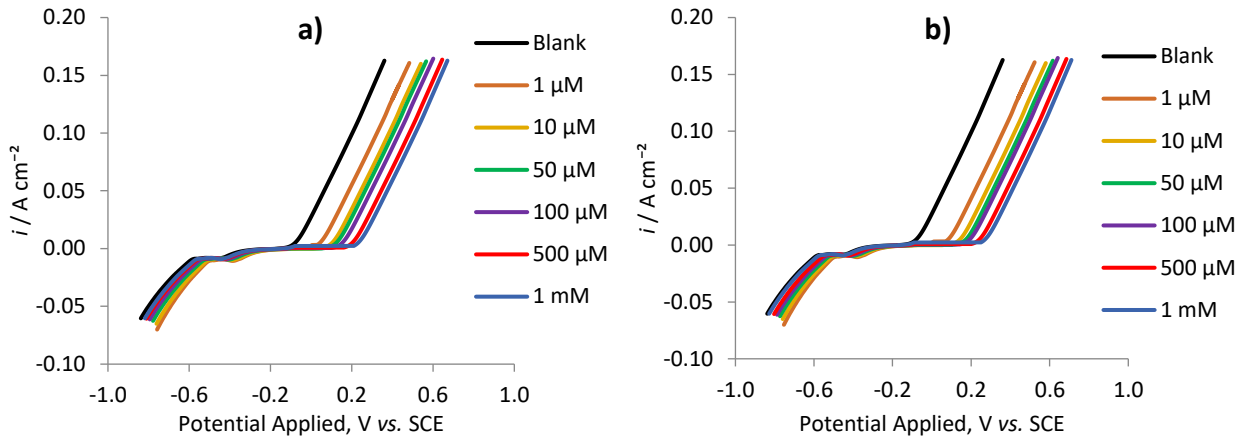

Figure 5. *Potentiodynamic anodic polarization curves for C12510 alloy in (1.0 M H_2SO_4 + 0.5 M NaCl) solution with various concentrations of a) m-TMPP and b) p-TMPP, at scan rate 0.1 mV s^{-1} and 298 K*

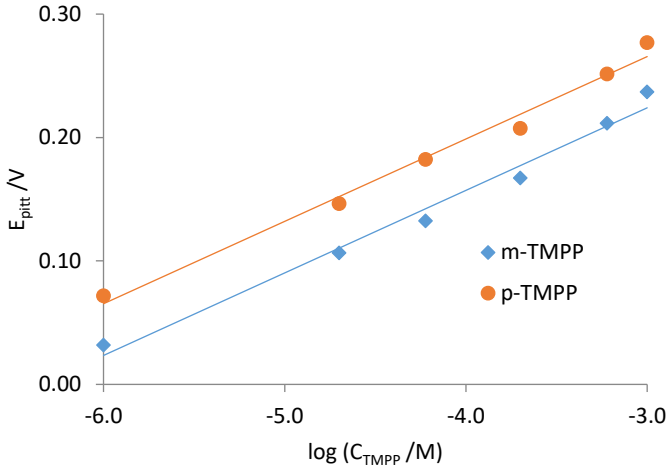

Figure 6. E_{pitt} vs. *log* C_{TMPP} *for C12510 alloy in (1.0 M H_2SO_4 + 0.5 M NaCl) solution with concentrations of TMPP, at scan rate 0.1 mV s^{-1} and 298 K*

These findings verify that the presence of TMPP molecules increases the resistance to pitting corrosion. These molecules are categorized as inhibitors of pitting corrosion. The noble shift of E_{pitt}, which suggests a greater ability to resist pitting corrosion, is greater for p-TMPP molecule than m-TMPP molecule at all concentrations tested.

Scanning electron microscopy analysis

The SEM is one of the most crucial instruments for surface analysis because of its capacity to offer a detailed microscopic view of metal surfaces. Figure 7 displays the SEM images of the surface of C12510 after PAP curves at a scan rate of 0.1 mV s^{-1} in (a) 1.0 M H_2SO_4, (b) 1.0 M H_2SO_4 + 0.5 M NaCl, (c) 1.0 M H_2SO_4 + 0.5 M NaCl + 0.001 M m-TMPP and (d) 1.0 M H_2SO_4 + 0.5 M NaCl + 0.001M p-TMPP. It can be noticed in Figure 7a that the unsmooth surface was produced by the corrosion attack of H_2SO_4 solutions. Figure 7b shows that when 0.5 M NaCl was added as a pitting corrosion agent, the C12510 surface became more damaged and the pits can be clearly observed. By introducing the m-TMPP and p-TMPP molecules into the corrosive system (Figure 7c and d), the surface of C12510 is improved and the pits observed in the presence of NaCl disappeared. Pitting corrosion is avoided because the TMPP compound adsorbs on the surface of C12510 and creates a surface layer that separates the C12510 apart from the aggressive solution. It is evident that p-TMPP molecules form a good film on the C12510 surface with a higher inhibition efficiency and less damage caused by

corrosion than the film formed by m-TMPP molecules. This last film shows lower inhibition efficiency than p-TMPP, and some corrosion damage still happens.

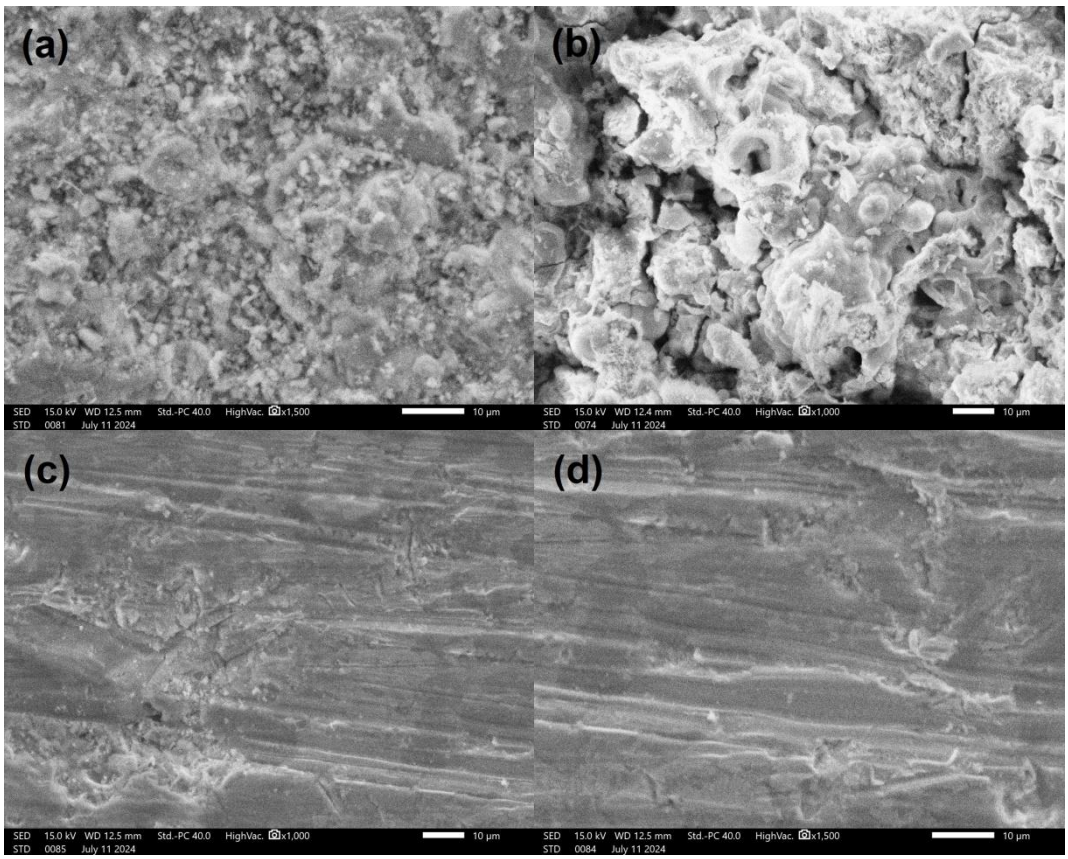

Figure 7. *SEM images for C12510 alloy in (a) 1.0 M H_2SO_4, (b) 1.0 M H_2SO_4 + 0.5 M NaCl, (c) 1.0 M H_2SO_4 + 0.5 M NaCl + 0.001 M m-TMPP and (d) 1.0 M H_2SO_4 + 0.5 M NaCl + 0.001 M p-TMPP*

Electrochemical impedance spectroscopy

Electrochemical impedance spectroscopy (EIS) is a non-invasive technique helpful for understanding the electrochemical corrosion process of the metal and how organic molecules affect the reaction mechanism and prevent the metal dissolution [25,26]. This method effectively clarifies the electrolyte-electrode interface dynamics, providing insight into various physical and chemical properties, such as metal surface roughness and impurities [27]. The Nyquist and Bode plots for the C12510 electrode in a blank 1.0 M H_2SO_4 and with certain concentrations of m-TMPP and p-TMPP molecules ranging from 1 μM to 1 mM are presented in Figure 8.

The measured Nyquist impedance graphs shown in Figure 8A display imperfect, not ideal semicircles. This is typically explained by the frequency dispersion of interfacial impedance arising from contaminants, surface roughness, grain boundaries, inhibitor adsorption, building up porous layers, and electrode surface homogenates. Also, the semicircles for the C12510 electrode, in the absence and presence of the TMPP compounds, are similar, implying that the TMPP inhibitors do not affect the corrosion mechanism, as previously reported by PP measurements [28]. The semicircular appearance seen in both blank 1.0 M H_2SO_4 solution and the presence of TMPP molecules claim that, in all cases, the charge transfer process governs the dissolution process of the C12510 electrode [29]. With increasing the concentration of TMPP molecules, the diameter of the capacitive loop increases, signifying higher charge transfer resistance, which appears due to the improved strength of the adsorbed inhibiting film.

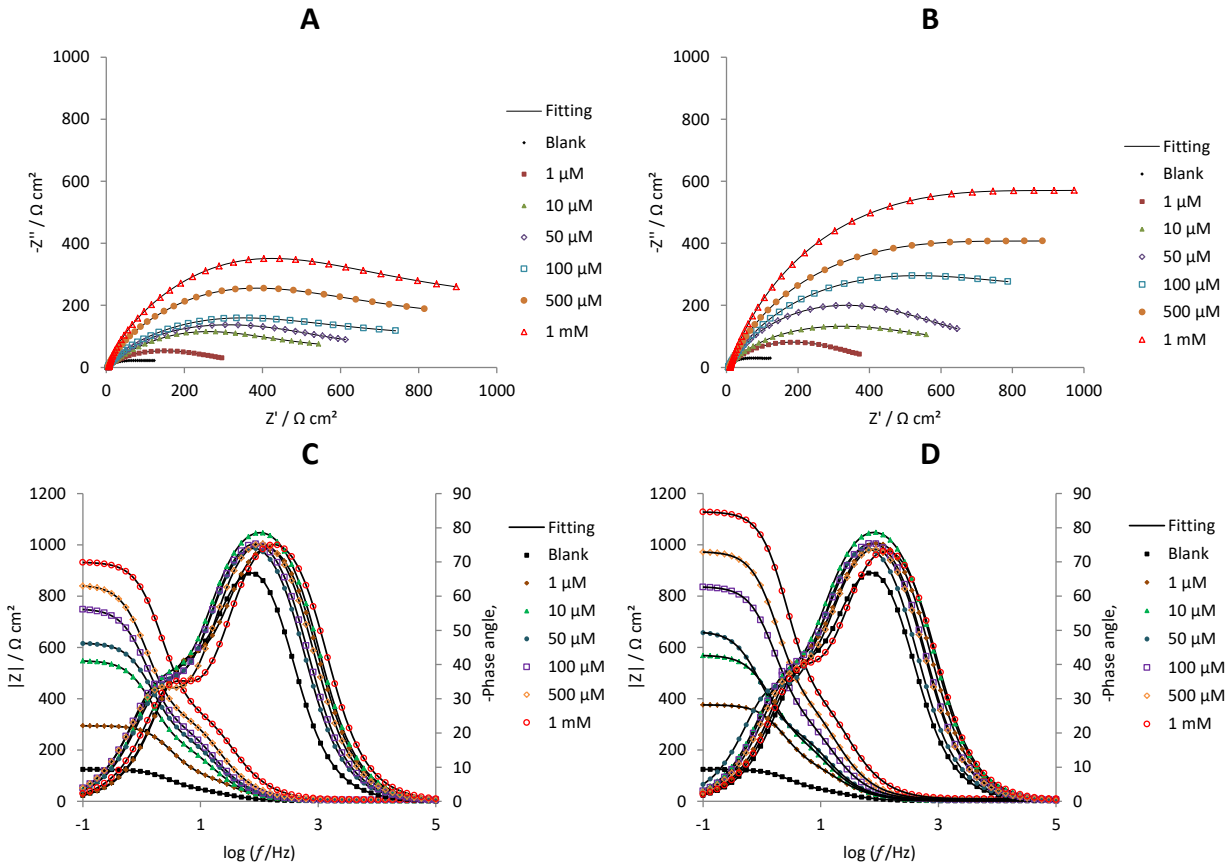

Figure 8. *The Nyquist and Bode plots for C12510 alloy in 1.0 M H_2SO_4 solution without and with different concentrations of (A and C) m-TMPP and (B and D) p-TMPP molecules*

Bode diagrams shown in Figure 8B represent the dependency of impedance modulus $|Z|$ and phase shift on frequency. Bode plots show clear separation into two time constants, indicated by the appearance of a change in slope of impedance modulus $|Z|$ and two phase angle maxima, effectively splitting the Bode plots into two sections, one at higher and another at lower frequencies. The impedance modulus increases with increasing the concentration of TMPP molecules, indicating the adsorption of TMPP molecules on the C12510 surface and strengthening the inhibitory effect against the H_2SO_4 solution [30]. Generally, higher concentrations of TMPP shift the phase-angle peaks to higher values, approaching the ideal capacitor values (-90°), an indication of their ordered distribution on the copper surface.

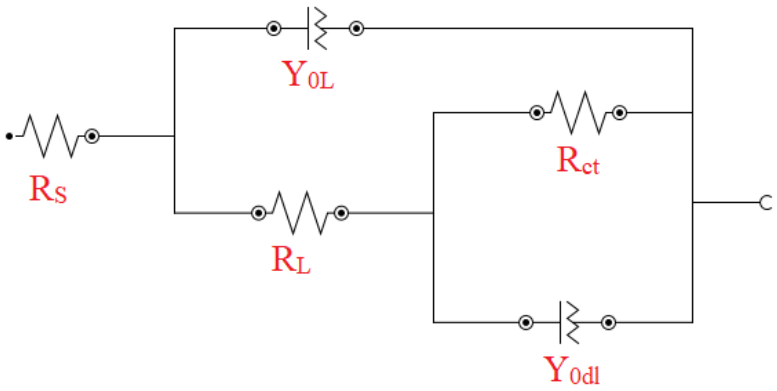

Figure 9. *The electrical equivalent circuit used to fit electrochemical impedance data of C12510 alloy*

The proposed electrical equivalent circuit designed for interpreting the impedance information is demonstrated in Figure 9. The recommended electrical equivalent circuit looks like this: initially, the

solution creates a resistance (R_S), followed by the impedance of an electrical double layer(Y_{0dl}) created by the corrosive solution in contact with the copper surface. Resistance to copper dissolution is denoted by charge transfer resistance (R_{ct}). Eventually, a chemical reaction occurs on the surface and chemical deposits are formed on the surface, creating a layer resistance (R_L), which arises from the formation of a barrier layer that impedes charge transfer during the electrochemical reaction. The capacitance of the barrier layer (Y_{0L}) is created with deposits acting as dielectrics. This phenomenon is supported by the PP results, as shown by the drops in the copper alloy's anodic and cathodic current densities at some potentials.

Table 2 summarizes impedance parameter values obtained by fitting the electrical equivalent circuit in Figure 9 to impedance spectra in Figure 8. The chi-square values (χ^2) are in the range of 10^{-4}, suggesting the consistency of the simulation and experimental data. As shown in Table 2, when TMPP concentrations are raised, both R_{ct} and R_L increase, most likely due to the adsorption of TMPP molecules on the C12510 surface, ongoing with the formation of a barrier layer of the inhibitor molecules on the C12510/electrolyte interface, inhibiting the electrochemical corrosion reaction, hence η_{EIS} rises [31].

Table 2. *AC impedance data for C12510 alloy in 1.0 M H_2SO_4 solution at room temperature with and without various TMPP concentrations*

	C / μM (at 298 K)	χ^2	R_S / Ω cm^2	n_{Y0dl}	Y_{0dl} / mS s^n cm^{-2}	C_{dl} / mF cm^{-2}	R_{ct} / Ω cm^2	n_{Y0L}	Y_{0L} / mS s^n cm^{-2}	R_L / Ω cm^2	η_{EIS}
Blank		0.00015	2.17	0.61	18.93	527.58	63.05	0.54	1.10	49.48	-
m-TMPP	1	0.00024	2.52	0.62	4.81	122.62	453.41	0.54	0.55	73.95	86.09
	10	0.00011	2.54	0.61	4.17	116.89	583.73	0.56	0.47	172.67	89.20
	50	0.00090	5.75	0.64	3.98	90.55	616.23	0.59	0.37	205.69	89.77
	100	0.00054	5.47	0.65	3.93	77.19	707.71	0.52	0.33	238.15	91.09
	500	0.00032	6.01	0.66	3.81	68.62	850.25	0.57	0.23	282.08	92.58
	1000	0.00041	6.61	0.68	1.89	28.16	905.41	0.57	0.13	290.52	93.04
p-TMPP	1	0.00032	2.96	0.58	8.94	334.44	492.13	0.57	0.64	105.34	87.19
	10	0.00018	2.86	0.58	7.20	252.72	622.09	0.59	0.54	188.96	89.86
	50	0.00032	6.10	0.59	6.04	210.37	777.34	0.54	0.45	228.93	91.89
	100	0.00041	6.45	0.61	5.07	144.49	811.44	0.50	0.34	249.23	92.23
	500	0.00076	9.33	0.60	4.41	131.72	935.81	0.58	0.24	298.33	93.26
	1000	0.00037	10.27	0.67	3.99	65.70	1085.88	0.55	0.14	307.55	94.19

True double-layer (C_{dl}) capacitance values were estimated by the following formula [32]:

$$C_{dl} = Y_{0dl}\omega^{n-1} = Y_{0dl}(2\pi f_{max})^{n-1} \quad (10)$$

where Y_{0dl} / S s^n cm^{-2} is a parameter that describes the impedance of constant phase element (CPE), applied instead of a true double layer capacitor described by C_{dl} / F cm^{-2} capacitance, n is CPE exponent, $\omega = 2\pi f$ is radial frequency, while f_{max} is the frequency at which the imaginary component of the impedance is maximal.

C_{dl} values decrease with increasing TMPP concentration. These TMPP molecules could replace water molecules at the C12510/electrolyte interface, increasing its surface coverage and effectively shielding the copper from the corrosive surroundings. This led to increased double-layer thickness and a drop in C_{dl}. The calculated η_{EIS} increases in the order p-TMPP > m-TMPP, as expected from the PP.

Weight loss technique

The corrosion behaviour of the C12510 sample was examined using the WL method at various concentrations of m-TMPP and p-TMPP molecules, ranging from 1 μM to 1 mM, and across a variety of time intervals, from 2 to 24 hours. The results gathered for the m-TMPP and p-TMPP molecules

are listed in Table 3. According to Table 3, the addition of two studied compounds greatly lowered the corrosion rate of C12510 in the acid solution and enhanced inhibition efficiency (η_W). Therefore, it is reasonable to conclude that the two tested compounds are effective in preventing acid corrosion of C12510.

Table 3. *Corrosion rates and inhibition efficacy of C12510 alloy in 1.0 H_2SO_4 solution with and without different TMPP concentrations for different immersion times*

Inhibitor	Time, h	Inhibitor concentration, μM												
		0	1		10		50		100		500		1000	
		CR_W/ mg cm^{-2} h^{-1}	CR_W/ mg cm^{-2} h^{-1}	η_W/ %	CR_W/ mg cm^{-2} h^{-1}	η_W/ %	CR_W/ mg cm^{-2} h^{-1}	η_W/ %	CR_W/ mg cm^{-2} h^{-1}	η_W/ %	CR_W/ mg cm^{-2} h^{-1}	η_W/ %	CR_W/ mg cm^{-2} h^{-1}	η_W/ %
m-TMPP	2	1.45	1.33	8.28	1.24	14.48	1.12	22.76	0.97	33.10	0.85	41.38	0.65	55.17
	4	2.61	2.22	14.94	2.06	21.07	1.7	34.87	1.38	47.13	0.85	67.43	0.44	83.14
	6	3.42	2.8	18.13	2.51	26.61	2.15	37.13	1.62	52.63	0.95	72.22	0.53	84.50
	8	4.72	3.26	30.93	3.03	35.81	2.5	47.03	1.88	60.17	1.1	76.69	0.62	86.86
	10	5.63	3.57	36.59	3.32	41.03	2.74	51.33	2.06	63.41	1.21	78.51	0.68	87.92
	20	7.4	3.56	51.89	3.31	55.27	2.73	63.11	2.05	72.30	1.2	83.78	0.68	90.81
	24	8.16	3.58	56.13	3.33	59.19	2.75	66.30	2.07	74.63	1.21	85.17	0.68	91.67
p-TMPP	2	1.45	1.31	9.66	1.18	18.62	1.12	22.76	0.91	37.24	0.78	46.21	0.5	65.52
	4	2.61	2.12	18.77	1.81	30.65	1.57	39.85	1.16	55.56	0.7	73.18	0.43	83.52
	6	3.42	2.47	27.78	2.12	38.01	1.83	46.49	1.35	60.53	0.79	76.90	0.39	88.60
	8	4.72	2.98	36.86	2.55	45.97	2.21	53.18	1.63	65.47	0.96	79.66	0.47	90.04
	10	5.63	3.33	40.85	2.85	49.38	2.47	56.13	1.82	67.67	1.07	80.99	0.52	90.76
	20	7.4	3.44	53.51	2.95	60.14	2.55	65.54	1.88	74.59	1.1	85.14	0.54	92.70
	24	8.16	3.39	58.46	2.91	64.34	2.51	69.24	1.86	77.21	1.09	86.64	0.53	93.50

The results demonstrate that the η_W increases as TMPP concentration and immersion time increase. This finding could be attributed to the fact that more molecules are adsorbed, covering a larger surface area of the C12510 as the TMPP concentration increases. Consequently, the corrosion rate is reduced, and the inhibition efficiency increases. It's noteworthy to observe that there is a small range in which the η_W increases from the lowest to the greatest TMPP concentration. This behaviour is due to the formation of an isolating layer resulting from the adsorption of TMPP molecules on the C12510 surface. The η_W is of the order: p-TMPP > m-TMPP. Also, there is an obvious agreement between η_W values obtained using weight loss data and those obtained with the PP, PAP and EIS techniques.

Activation thermodynamic parameters

The influence of raising the temperature on the corrosion of C12510 in blank 1.0 M H_2SO_4 and inhibited by 1 mM m-TMPP and p-TMPP compounds for 2 h, was examined at temperatures ranging from 298 to 343 K. The calculated results presented in Table 4 show that with increasing temperature the values of CR_W rise, while the η_W are reduced. A decrease in the % η_W and an increase in the rate of elimination of the adsorbed TMPP from the surface of C12510 support the physical adsorption of the TMPP compounds on the C12510 surface.

The activation energy (E_a), the activation enthalpy (ΔH^*), and the activation entropy (ΔS^*) of C12510 in blank 1.0 M H_2SO_4 and solution containing 1 mM m-TMPP and p-TMPP molecules for 2 hours were assessed using Arrhenius equation and transition state relation [33]:

$$\ln CR_W = \ln A - \frac{E_a}{RT} \quad (11)$$

$$\ln\left(\frac{CR_W}{T}\right) = \left[\ln\left(\frac{R}{N_A h}\right) + \frac{\Delta S^*}{R}\right] - \frac{\Delta H^*}{RT} \quad (12)$$

where, A is the Arrhenius constant, h is the Planck's constant and N_A is Avogadro's number.

Table 4. *Thermodynamic activation parameters of C12510 alloy in 1.0 M H_2SO_4 solution both with and without 1 mM TMPP in different temperatures after 2 h of immersion time*

Solution	T / K	CR_W / mg cm^{-2} h^{-1}	η_W / %	E_a / kJ mol^{-1}	ΔH^* / kJ mol^{-1}	ΔS^* / J mol^{-1} K^{-1}
1 M H_2SO_4	298	1.45	-	26.42	23.76	-162.16
	313	2.31	-			
	323	3.33	-			
	333	4.84	-			
	343	5.48	-			
1 M H_2SO_4 + 1 mM m-TMPP	298	0.65	54.88	37.89	35.24	-130.42
	313	1.23	46.82			
	323	2.09	37.17			
	333	3.68	24.07			
	343	4.36	20.43			
1 M H_2SO_4 + 1 mM p-TMPP	298	0.50	65.17	38.90	36.25	-128.65
	313	1.17	49.42			
	323	1.77	46.97			
	333	2.94	39.26			
	343	3.84	29.98			

Figures 10A and 10B exhibit the plots of log CR_W and log (CR_W/T) *vs*. 1/T for the C12510 sample in blank 1.0 M H_2SO_4 and with 1 mM concentrations of m-TMPP and p-TMPP molecules. Straight lines were produced with a coefficient of determination (R^2) close to unity.

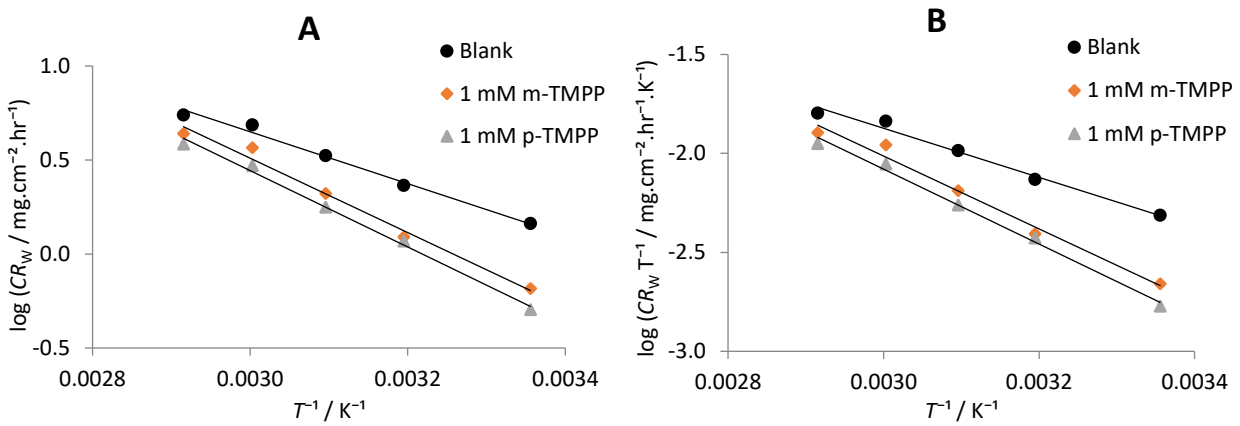

Figure 10. *Arrhenius (A) and transition state (B) plots for C12510 alloy in 1.0 M H_2SO_4 solution with and without 1 mM concentrations of m-TMPP and p-TMPP*

From the slope of the straight lines in Figure 10A, the values of E_a were computed and listed in Table 4. In the presence of TMPP molecules, the values of E_a are greater than in blank 1.0 M H_2SO_4, suggesting the physical adsorption of TMPP molecules on the C12510 sample. The higher value of E_a in the presence of TMPP molecules denotes the creation of a higher energy barrier against the corrosion process because an adsorbed layer has developed on the C12510 surface [34]. From the slopes and the intercepts of the straight lines in Figure 10B, the values of ΔH^* and ΔS^* were computed and listed in Table 4. The positive values of ΔH^* values imply an endothermic corrosion reaction, and when TMPP is added, the value rises, which suggests a greater need for heat for the reaction to proceed. The activated complex of the rate-determining step is association instead of dissociation, as indicated by the negative entropy change (ΔS^*) sign, which represents the formation of more arrangement when the reactant transforms to the activating complex.

Adsorption isotherm

Applying weight loss data, the surface coverage (θ) was determined for the varied concentrations of TMPP molecules to analyse the adsorption behaviour of TMPP on C12510 in 1.0 M H_2SO_4 solution.

The adsorption process can be thought of as an exchange process between the TMPP molecules in the aqueous solution [$TMPP_{(aq.)}$] and water molecules adsorbed on the C12510 [$H_2O_{(ads)}$] to donate the adsorbed TMP on the C12510 surface [$TMPP_{(ads.)}$], using Equation (13):

$$TMPP_{(aq.)} + H_2O_{(ads.)} \rightarrow TMPP_{(ads.)} + \beta H_2O_{(aq.)} \quad (13)$$

where β is the amount of water molecules exchanged by one TMPP molecule.

The interaction between the C12510 surface and TMPP molecules in 1.0 M H_2SO_4 solution is studied through the adsorption isotherm. The surface coverage value (θ) estimated from the WL technique is employed for several adsorption isotherms. It was found that the Langmuir isotherm matches the experimental data excellently, according to the following equation:

$$\frac{C_{TMPP}}{\theta} = \frac{1}{K_{ads}} + C_{TMPP} \quad (14)$$

where K_{ads} / M^{-1} is the equilibrium constant of adsorption.

Straight lines were obtained by plotting C_{TMPP}/θ versus C_{TMPP} with correlation coefficient (R^2) close to 1.0 as shown in Figure 11. The value of K_{ads} computed from the intercept reveals that a monolayer of TMPP molecules is formed on the C12510 surface with no side interactions between the adsorbed particles.

The standard free energy of adsorption (ΔG^o_{ads}) was estimated from Equation (15) [35]:

$$\Delta G^o_{ads} = -RT \ln (55.5 K_{ads}) \quad (15)$$

where 55.5 is the molarity of water. The calculated values of ΔG^o_{ads} at all tested hours are negative, revealing that the TMPP molecules adsorb on the C12510 surface spontaneously, Table 5.

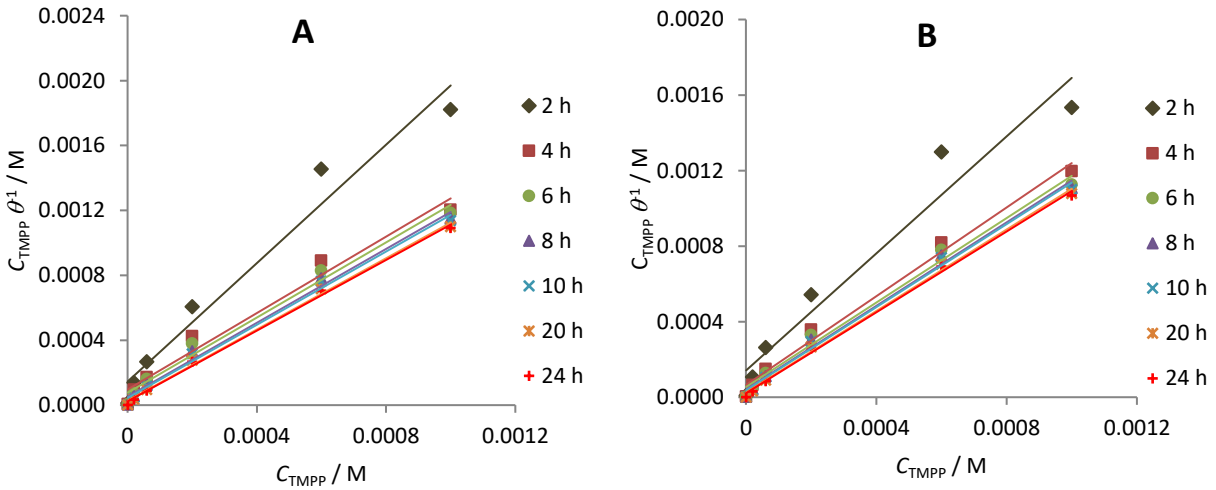

Figure 11. *Langmuir adsorption isotherm for (A) m-TMPP and (B) p-TMPP on C12510 alloy in 1.0 M H_2SO_4 solution after different immersion times at 298 K*

Also, it is known that the higher ΔG^o_{ads} negative value, the more effective adsorption is. The values of ΔG^o_{ads} ranged from -31.86 to -36.63 kJ mol^{-1} and the high K_{ads} seen in the Langmuir model demonstrate that TMPP inhibitors are adsorbed on copper surfaces through a combination of physical and chemical adsorption process. The negative values of ΔG^o_{ads}, after immersion for 2 hours through 24 hours for p-TMPP, range from -31.93 to -36.63 kJ mol^{-1} and are somewhat larger than those for m-TMPP ranging from -31.86 to -36.38 kJ mol^{-1}, which is expected from weight loss measurements above. p-TMPP may show flatness and better spreading on the copper surface, which is reflected in the higher adsorption efficiency.

Table 5. *The equilibrium constant and adsorption standard free energy of various concentrations of TMPP on C12510 alloy in 1.0 M H_2SO_4 solution at room temperature*

Inhibitor	Time, h	R^2	K_{ads} / mM^{-1}	ΔG_{ads} / kJ mol^{-1}
m-TMPP	2	0.9654	6.91	-31.86
	4	0.9741	10.389	-32.87
	6	0.9845	13.088	-33.44
	8	0.9910	19.203	-34.39
	10	0.9930	22.820	-34.82
	20	0.9966	37.109	-36.03
	24	0.9973	42.756	-36.38
p-TMPP	2	0.9477	7.103	-31.93
	4	0.9893	15.552	-33.87
	6	0.9890	18.723	-34.33
	8	0.9925	24.308	-34.98
	10	0.9937	27.252	-35.26
	20	0.9966	40.161	-36.22
	24	0.9974	47.287	-36.63

Inhibition mechanism

The inhibition of corrosion performance of the C12510 sample in blank 1.0 M H_2SO_4 by the TMPP molecules using WL, PP, PAP, and EIS methods was found to depend on the concentration, kind and the position of the substitutes group in the molecule. The adsorption characteristics can be used to understand the nature of the inhibitor interaction on the metal surface during corrosion inhibition. The findings demonstrate that adsorption of the inhibitor at the solution interface inhibits corrosion. Some factors that influence the inhibitory efficacy of additive compounds are the amount of adsorption active sites and their charge density, the size of the molecule, the adsorption process, and the creation of metallic complexes.

The interaction between the TMPP molecule and C12510 surface ions may cause the stable complex to develop by forming four coordination bonds between the copper ion and the electron lone pairs of nitrogen atoms. The proposed structures of the complexes are presented in Figure 12. The results obtained from many methodologies in this study verify that p-TMPP has a somewhat higher inhibition efficiency order than m-TMPP. The molecular structure of the two TMPP compounds contains four methoxy groups (−OCH_3), contributing to their strong inhibitory efficacy. The methoxy group exhibits a negative inductive effect (−I) and a positive mesomeric impact (+M). The methoxy group's Hammett constant [36] is equivalent to σ = −0.27, which intensifies the molecule's delocalized π electrons. This group raises the molecule's electron charge density, increasing the inhibition efficiency.

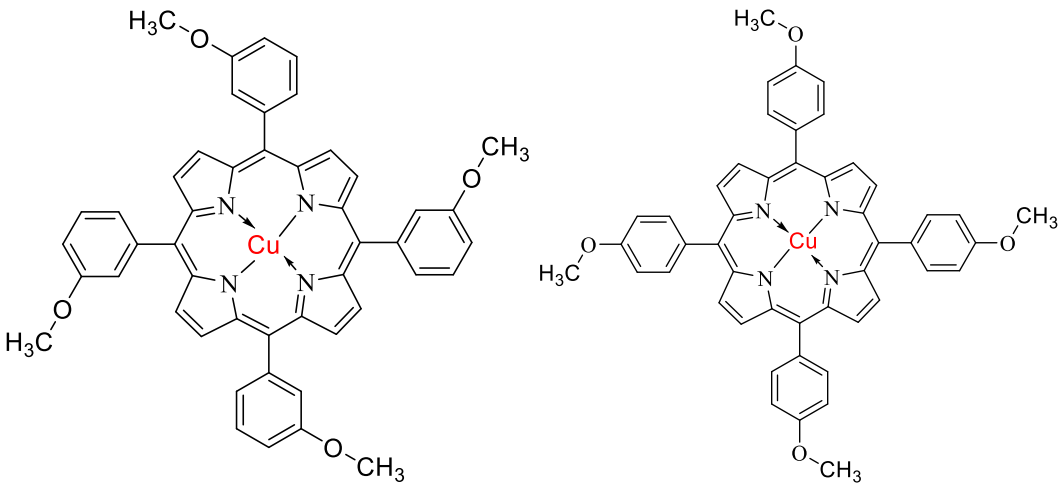

Figure 12. *The proposed structures of the complex formed between copper ion and TMPP molecule*

According to earlier findings on inhibition efficiency obtained from various methods, p-TMPP has a higher inhibition efficiency order than m-TMPP. The p-substituted group's inductive and mesomeric actions work in harmony to raise the degree of surface coverage and, as a result, the inhibitory efficiency. The efficacy of inhibition in the case of m-substituted groups depends on the resonance and inductive effects (+R, -I), which alter the electron density and activate the aromatic ring.

Density functional theory study

Theoretical calculations were conducted to complement experimental findings and provide insight at the molecular level. Among the available quantum chemical techniques for analysing corrosion inhibitors, density functional theory (DFT) has proven highly effective in identifying changes in the electronic structure that contribute to the inhibition mechanism. Recent advancements in DFT have enhanced its ability to accurately predict molecular properties and describe atomic interactions within molecules. Over the past decade, DFT has gained widespread popularity due to its precision and efficient use of computational resources, making it an invaluable tool for corrosion studies [37]. Figure 13 shows the optimized geometries of m-methoxy tetraphenyl porphyrin (m-TMPP) and p-methoxy tetraphenyl porphyrin (p-TMPP). The difference in the position of the methoxy group between the meta and para configurations results in slightly altered molecular geometries. The geometry optimization indicates that both structures retain the planar nature typical of porphyrins, but the subtle differences in bond angles and orientations of the phenyl groups are likely to influence the electronic properties of each molecule.

m-methoxy tetraphenyl porphyrin (m-TMPP) p-methoxy tetraphenyl porphyrin (p-TMPP)

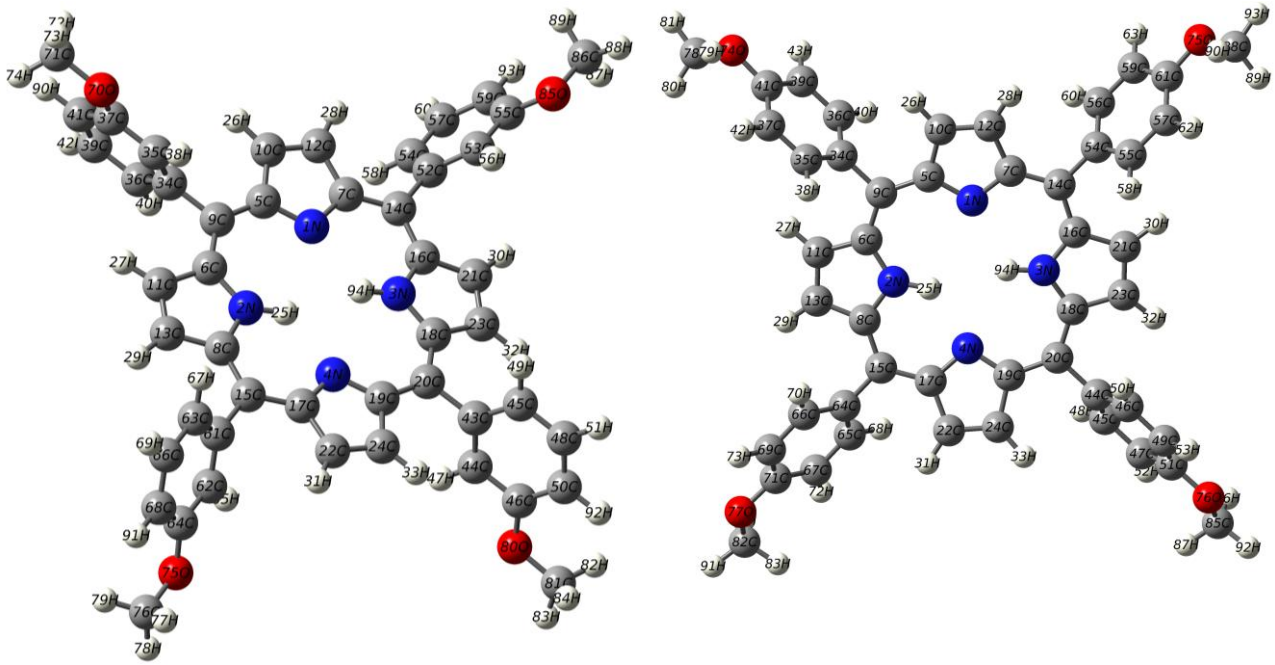

Figure 13. *Optimized geometries of m-TMPP and p-TMPP molecules*

In Figure 14, the LUMO (lowest unoccupied molecular orbital) and HOMO (highest occupied molecular orbital) maps, as well as the ESP (electrostatic potential) maps, are presented for m-TMPP and p-TMPP. The frontier orbitals play a significant role in determining the reactivity and interaction with surfaces or molecules. The HOMO for both m-TMPP and p-TMPP appears localized on the porphyrin ring, indicating that this area is responsible for electron donation. The LUMO, on the other hand, is slightly more delocalized, allowing for electron acceptance over a broader region. The ESP

maps show regions of electron-rich and electron-deficient areas, which are crucial for understanding intermolecular interactions. The different methoxy positions (meta *vs*. para) shift the electron density slightly, which may explain the differences in chemical reactivity.

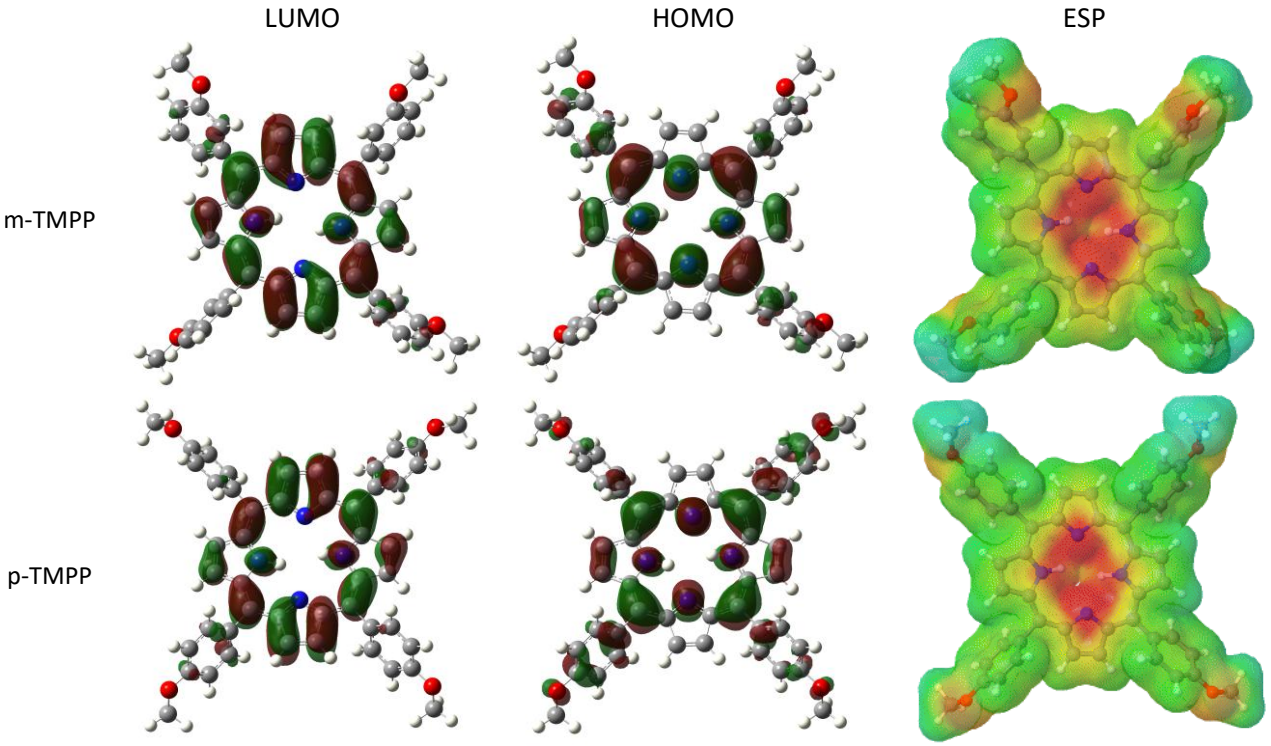

Figure 14. *Frontier orbitals and ESP maps of m-TMPP and p-TMPP*

The dipole moment vectors indicate the magnitude and direction of the molecular dipole. As shown in Figure 15, for m-TMPP, the dipole moment is relatively small at 0.79 debye, indicating that the electron distribution is relatively symmetrical. In contrast, p-TMPP shows a much larger dipole moment of 3.51 debye, suggesting a greater asymmetry in the charge distribution due to the para-substitution of the methoxy group. This difference in dipole moments is significant, as a larger dipole moment can influence the interaction with polar environments and surfaces. p-TMPP has a larger dipole moment than m-TMPP, as indicated by both experimental results and DFT calculations.

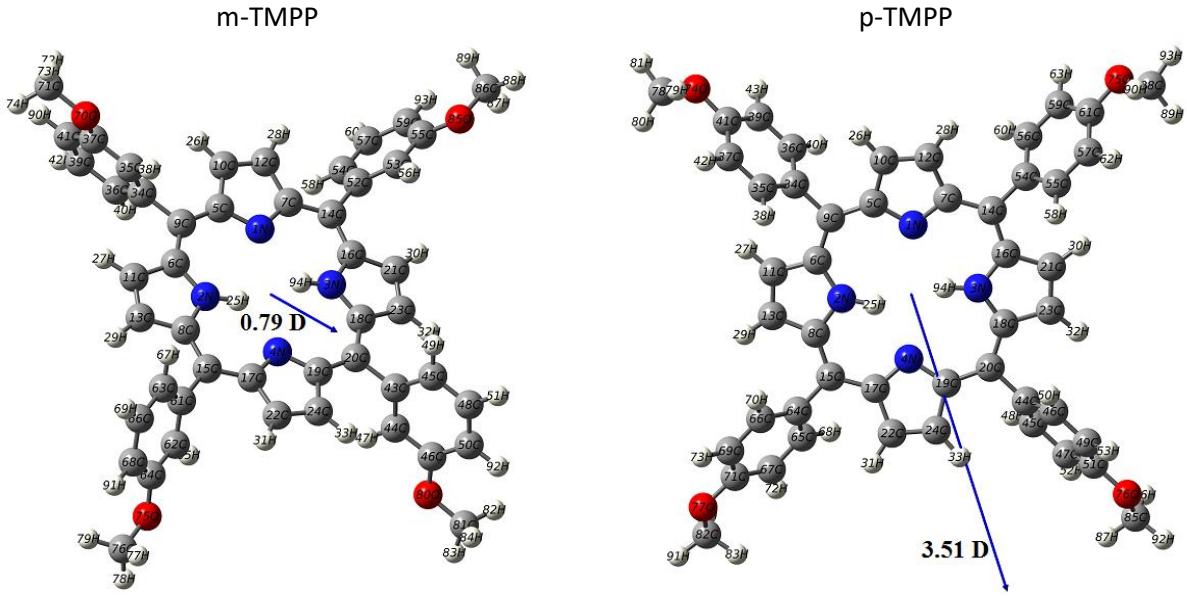

Figure 15. *Dipole moment vectors for m-TMPP and p-TMPP*

The larger dipole moment in p-TMPP increases its polarity, resulting in stronger electrostatic interactions between the inhibitor and the charged copper surface in acidic H_2SO_4 media. p-TMPP effectively reduces the rate of copper corrosion by creating a thicker and more protective adsorption layer as a result of the enhanced attraction. The quantum parameters for both m-TMPP and p-TMPP, as presented in Table 6, are essential for understanding their electronic properties. The energies of the frontier orbitals (E_{HOMO} and E_{LUMO}) provide key insights into the interaction between molecules and a copper surface. A higher E_{HOMO} indicates a greater ability for a molecule to donate electrons, which enhances its interaction with metal surfaces. In contrast, E_{LUMO} reflects the molecule's tendency to accept electrons; the lower the E_{LUMO}, the stronger its electron-accepting capability.

For m-TMPP and p-TMPP, the LUMO energy levels are -5.20 and -5.00 eV, respectively, while the HOMO levels are -2.58 eV for m-TMPP and -2.53 eV for p-TMPP as summarized in Table 6. These values indicate a subtle difference in electronic structure. The HOMO-LUMO gap is crucial in determining how well a molecule can interact with a metal surface. A smaller gap generally means a molecule can easily donate or accept electrons, facilitating stronger adsorption onto the metal. This process is key in forming a protective layer that prevents metal corrosion, especially in aggressive environments like acidic media (H_2SO_4). In this case, the slightly smaller band gap of p-TMPP as shown in Table 6, suggests a stronger affinity for the metal surface, thereby providing a better barrier against corrosive species compared to m-TMPP. In an aqueous phase, the protonation of p-TMPP and m-TMPP occurs on the nitrogen atom of the pyrrole unit, which carries the most negative charge. As seen in Figure 16, protonation decreases the energies of both frontier orbitals due to the increased electron-withdrawing nature of the positively charged pyrrole unit. However, the trend of p-TMPP having slightly higher HOMO and LUMO levels than m-TMPP remains consistent. Upon protonation, p-TMPP retains the smaller gap. The smaller band gap of p-TMPP in both protonated and non-protonated forms suggests a greater ease of electron transfer, which is critical for the formation of a robust protective barrier on the metal. This property makes p-TMPP more effective in environments such as acidic media.

The hardness and softness values of m-TMPP and p-TMPP are important indicators of their reactivity and inhibition efficiency in copper corrosion in H_2SO_4 media. Hardness (γ) is inversely related to a molecule's reactivity. A higher hardness value indicates that the molecule is more stable and less reactive, meaning it resists changes in its electronic configuration. Softness (σ), being the reciprocal of hardness, indicates how easily a molecule can donate or accept electrons.

Table 6. *Quantum parameters of m-TMPP and p-TMPP inhibitors*

Compound	LUMO, eV	HOMO, eV	ΔE / eV	Dipole moment, D	γ / eV	σ / eV^{-1}	Number of electrons transferred
m-TMPP	-5.20	-2.58	2.62	0.79	1.31	0.763	3.37
p-TMPP	-5.00	-2.53	2.47	3.51	1.235	0.810	3.52

A higher softness value suggests higher reactivity and a stronger ability to interact with external species, such as metal surfaces. As seen in Table 6, p-TMPP is softer and, therefore, more reactive, making it a better electron donor or acceptor. This enables it to interact more strongly with the copper surface, leading to better adsorption and a more effective inhibition layer. The higher reactivity of p-TMPP also allows it to respond more efficiently to changes in the local environment, improving its ability to prevent the penetration of aggressive ions. m-TMPP, being harder and less reactive, would be less effective in forming strong interactions with the copper surface. While it can still act as a corrosion inhibitor, its lower softness means that it would not adsorb as strongly as p-TMPP and its ability to block corrosive species will be diminished.

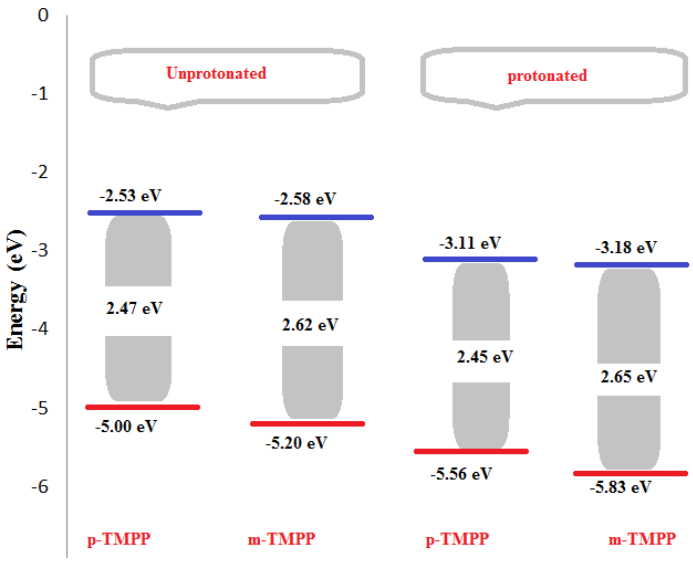

Figure 16. *Frontier orbitals of m-TMPP and p-TMPP in unprotonated and protonated forms*

The number of electrons transferred (Δ*N*) between the Cu surface and the inhibitor molecules m-TMPP and p-TMPP is a crucial indicator of how these molecules interact with the metal surface. According to Equation (7), the Δ*N* values represent the extent to which electrons are donated from the inhibitor molecules to the unoccupied 3d-orbitals of Cu, demonstrating their electron-donating capacity. As mentioned, positive Δ*N* values indicate that the inhibitors act as electron donors (or Lewis bases) [38]. Both m-TMPP and p-TMPP show positive Δ*N* values, which means they can donate electrons to the copper surface. This electron donation enhances the adsorption of the inhibitors on the copper surface, contributing to their ability to form a protective layer that inhibits corrosion. From Table 6, the Δ*N* values for m-TMPP and p-TMPP are 3.37 and 3.52 e, respectively. These values are less than 3.6 e, indicating moderate electron donation, but enough to create a strong interaction with the copper surface. The fact that p-TMPP has a slightly higher ΔN value than m-TMPP suggests that p-TMPP can transfer more electrons to the copper surface, making it a slightly more effective corrosion inhibitor.

Monte Carlo simulation

The adsorption of m-TMPP and p-TMPP on the Cu (111) surface was conducted to explore the interaction between the inhibitors and the copper surface. Figure 17 demonstrates the adsorption geometry of both molecules.

From the figure, it is evident that during the adsorption process, the inhibitors gradually approach the Cu (111) surface in a tilted orientation in the aqueous phase, with the phenyl methoxy groups pointing towards the copper surface. In the gas phase, both inhibitors adopt a parallel configuration, where the entire molecular plane aligns with the Cu (111) surface.

This specific orientation allows for increased surface coverage, as the phenyl methoxy groups enhance the adsorption of the molecules to the copper surface. The tilted configuration leads to a greater surface coverage compared to other orientations, which improves the overall inhibition efficiency (η). These findings align with previous discussions in this research, which suggest that better surface coverage leads to more effective corrosion protection. This interaction is also quantitatively illustrated in Table 7. The most stable configurations observed in the system are those associated with the lowest adsorption energies, indicating the most favourable adsorption interactions. The adsorption energy of p-TMPP is calculated to be -1120.73 kJ mol^{-1}, while m-TMPP

shows a slightly less negative adsorption energy of -1108.3 kJ mol^{-1}. These values indicate that both inhibitors have strong interactions with the surface, but p-TMPP demonstrates a stronger inhibitory efficiency due to its more negative adsorption energy.

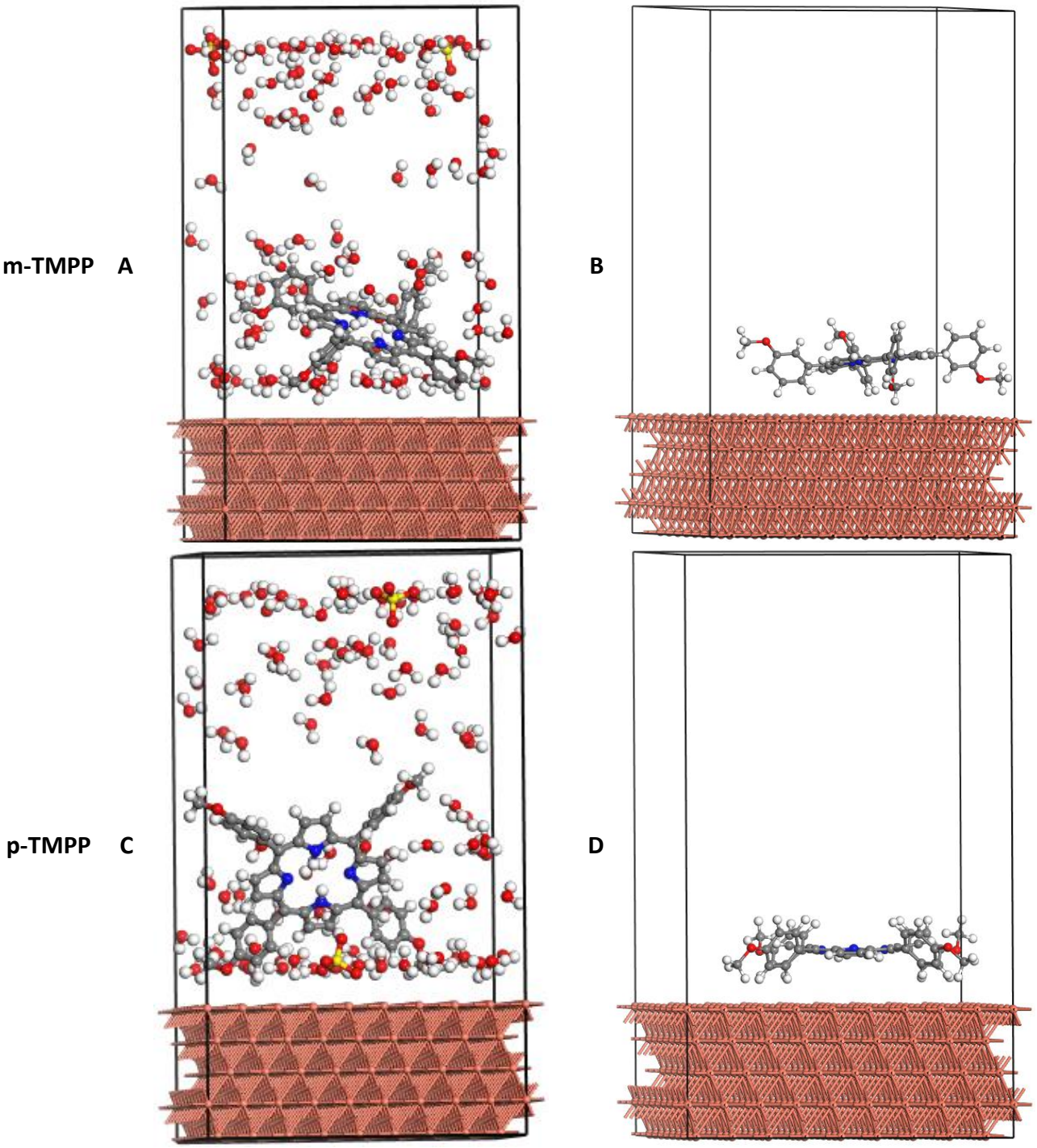

Figure 17. *Adsorption view of m-TMPP (A and B) and p-TMPP (C and D) on Cu (111) surface in aqueous (A and C) and gas (B and D) media*

Table 7. *Adsorption energy for m-TMPP and p-TMPP inhibitors on Cu (111) surface*

Phase	System	Adsorption energy, kJ mol^{-1}
Aqueous	m-TMPP + Cu (111)	-1108.3
	p-TMPP + Cu (111)	-1120.73
Gas	m-TMPP + Cu (111)	-406.308
	p-TMPP + Cu (111)	-520.866

This observation supports the results previously discussed, confirming the enhanced ability of p-TMPP to adsorb onto and protect the surface, likely due to better surface coverage and stronger interaction with the Cu (111) surface. The higher magnitude of adsorption energies in the aqueous phase indicates stronger adsorption interactions compared to the gas phase. The solvation effects in water enhance the stabilization of the inhibitor-metal complex. Among the two, p-TMPP exhibits slightly stronger adsorption than m-TMPP, suggesting better inhibitor performance.

Comparison with previous studies

Table 8 compares the inhibition efficiency (η) due to m-TMPP and p-TMPP compounds with some other inhibitors used as corrosion inhibitors for copper and copper alloys in H_2SO_4 solution. All these inhibitors had a high percentage of inhibition efficiency due to their strong adsorption onto the copper surface.

Table 8. *Comparison of the inhibition efficacy of m-TMPP and p-TMPP on copper alloy surface from the present work with some previous literature studies*

Inhibitor	Substrate	Corrosive medium	Optimal inhibitor concentration	η / %	Ref.
Glycine, tyrosine, , valine	Cu	O_2-saturated 0.50 M H_2SO_4	50 mM	98 for tyrosine, 91 for glycine and 75 for alanine and valine	[39]
Cauliflower extract	Cu	0.5 M H_2SO_4	400 ppm	99.0	[40]
Montelukast sodium	Cu	0.5 M H_2SO_4	50 ppm	99.0	[41]
Losartan potassium	Cu	0.5 M H_2SO_4	40 ppm	94.9	[42]
Capsicum annuum L. leaf extract	Cu	0.5 M H_2SO_4	500 ppm	93.9	[43]
m-TMPP	C12510 alloy	1.0 M H_2SO_4	1 mM	96.23	Current work
p-TMPP				97.61	

Conclusions

Two porphyrin molecules (m-TMPP and p-TMPP) provided efficient corrosion inhibition against copper alloy (C12510) in 1.0 M H_2SO_4 solution. Every technique (weight loss, potentiodynamic polarization, potentiodynamic anodic polarization, electrochemical impedance spectroscopy and Monte Carlo simulation) employed in the study confirmed the inhibitory potency of TMPP molecules. The inhibitory effectiveness of two TMPP molecules rose as their concentration increased and dropped with increasing temperature. The inhibitory mechanism was attributed to the spontaneous physicochemical adsorption of TMPP molecules onto the C12510 surface, as evidenced by the moderately high negative ΔG_{ads} values. According to the polarization data, these compounds exhibit mixed (cathodic and anodic) inhibitory action without affecting the corrosion mechanism. The adsorption of both inhibitor molecules matched Langmuir's isotherm properties. EIS approach demonstrated the charge transfer mechanism that governs metal dissolution (corrosion) reaction and the presence of the corrosion product layer on the copper alloy surface. In corrosive H_2SO_4 + NaCl solution, the TMPP molecules slowed the pitting corrosion, by shifting the pitting potential to a more noble direction. The inhibitory efficacy of p-TMPP is higher than m-TMPP at all concentrations tested. Also, this study highlights the utility of DFT and Monte Carlo simulations in evaluating the corrosion inhibition efficiency of organic inhibitors like m-TMPP and p-TMPP on copper surfaces. The results demonstrated that p-TMPP, with its higher dipole moment, lower HOMO-LUMO gap, and greater electron-donating ability, exhibits superior adsorption and interaction with the Cu (111) surface. This is further supported by the adsorption energies obtained

from Monte Carlo simulations, where p-TMPP shows stronger interaction with the copper surface compared to m-TMPP.

Acknowledgment*:The authors express their gratitude to Princess Nourah bint Abdulrahman University Researcher supporting project number (PNURSP2024R53). Princess Nourah bint Abdulrahman University, Riyadh, Saudi Arabia.*

References

[1] B. Tan, Y. Liu, Z. Gong, X. Zhang, J. Chen, L.-Guo, J.-Xiong, J.-Liu, R.-Marzouki, W.-Li, Pyracantha fortuneana alcohol extracts as biodegradable corrosion inhibitors for copper in H_2SO_4 media, *Journal of Molecular Liquids* **397** (2024) 124117. https://doi.org/10.1016/j.molliq.2024.124117

[2] H. T. Hossein, M. G. Hosseini, Corrosion inhibition of copper in Sulphuric acid by some nitrogen heterocyclic compounds, *Anti-Corrosion Methods and Materials* **54** (2007) 308-313. https://doi.org/10.1108/00035590710822161

[3] T. A. Farghaly, A. Fawzy, H. H. Alsharief, N. Alqarni, A. Al Bahir, S. M. Riyadh, Investigation of inhibition efficiencies of Novel *bis*-oxindole and *bis*(spiro(triazole-oxindole)) for the corrosion of copper in sulfuric acid medium, *Polycyclic Aromatic Compounds* **44** (2024) 1258-1272. https://doi.org/10.1080/10406638.2023.2191972

[4] R. N. Felaly, M. Alfakeer, A. A. I. Ali, S. S. Al-Juaid, E. M. Mabrouk, A.Y. El-Etre, D. F. Seyam, M. Abdallah, Enhanced corrosion protection of copper alloy in 2.0 M HNO_3 solution using expired solo sept, slim-lax and well derm drugs, *International Journal of Electrochemical Science* **19** (2024) 100657. https://doi.org/10.1016/j.ijoes.2024.100657

[5] A. S. Fouda, M. A. Ismail, M. A. Khaled, Experimental and computational chemical studies on the corrosion inhibition of new pyrimidinone derivatives for copper in nitric acid, *Scientific Reports* **12** (2022) 16089. https://doi.org/10.1038/s41598-022-20306-4

[6] E. E. El-Katori, A. S. Abousalem, Impact of some pyrrolidinium ionic liquids on copper dissolution behavior in acidic environment: experimental, morphological and theoretical insights, *RSC advances* **9** (2019) 20760-2077. https://doi.org/10.1039/C9RA03603B

[7] M. Abdallah, K.A. Soliman, M. Alshareef, A.S. Al-Gorair, H. Hawsawi, H.M. Altass, S.S. Al-Juaid, M.S. Motawea, Investigation of the anticorrosion and adsorption properties of two polymer compounds on the corrosion of SABIC iron in 1 M HCl solution by practical and computational approaches, *RSC Advances* **12** (2022) 20122–20137. https://doi.org/10.1039/D2RA03614B

[8] M. Abdallah, M. Alfakeer, Mubark Alshareef, H. Hawsawi, Salih S. Al-Juaid, R.S. Abdel Hameed, M. Sobhi, Natural Sweet Almond Oil as an Effective Green Inhibitor for Aluminum Corrosion in Sulfuric Acid Medium, *International Journal of Electrochemical Science* **17** (2022) 220949. https://doi.org/10.20964/2022.09.18

[9] A. Fouda, H. Abdel-Wahed, M. Atia, A. El-Hossiany, Novel porphyrin derivatives as corrosion inhibitors for stainless steel 304 in acidic environment: synthesis, electrochemical and quantum calculation studies, *Scientific Reports* **13** (2023) 17593. https://doi.org/10.1038/s41598-023-44873-2

[10] A. Singh, Y. Lin, M. A. Quraishi, L. O. Olasunkanmi, O. E. Fayemi, Y. Sasikumar, B. Ramaganthan, I. Bahadur, I. B. Obot, A. S. Adekunle, Porphyrins as corrosion inhibitors for N80 steel in 3.5% NaCl solution: electrochemical, quantum chemical, QSAR and Monte Carlo simulations studies, *Molecules* **20** (2015) 15122-15146. https://doi.org/10.3390/molecules200815122

[11] A. D. Adler, F. R. Longo, J. D. Finarelli, J. Goldmacher, J. Assour, L. Korsakoff, A simplified synthesis for meso-tetraphenylporphine, *The Journal of Organic Chemistry* **32** (1967) 476-476. https://doi.org/10.1021/jo01288a053

[12] R. Dennington, T. A. Keith, J. M. Millam, GaussView 6.0. 16, *Semichem Inc.: Shawnee Mission, KS, USA* (2016) 143-150. https://gaussian.com/gaussview6/

[13] A. S. Al-Gorair, T. Al-Habal, R. El-Sayed, S. S. Al- Juaid, R. S. Abdel Hameed, M. Abdallah, Investigations of non-ionic surfactants derived from triazoles and pyrroles as potent corrosion inhibitors for carbon steel in hydrochloric acid, *International Journal of Electrochemical Science* **18 (9)** (2023) 100269. https://doi.org/10.1016/j.ijoes.2023.100269

[14] A. D. Adler, F. R. Longo, W. Shergalis, Mechanistic Investigations of Porphyrin Syntheses. I. Preliminary Studies on *ms*-Tetraphenylporphin, *Journal of the American Chemical Society* **86** (1964) 3145-3149. https://doi.org/10.1021/ja01069a035

[15] A. B. Nielsen, A. J. Holder, GaussView 5 Reference. Gaussian Inc., Pittsburgh, USA, 2009. https://chemistry4.me/Gaussian/G09W/gvref/gv5ref.pdf

[16] M. J. Frisch, G. W. Trucks, H. B. Schlegel, G. E. Scuseria, M. A. Robb, J. R. Cheeseman, G. Scalmani, V. Barone, B. Mennucci, G. A. Petersson, H. Nakatsuji, M. Caricato, X. Li, H. P. Hratchian, A. F. Izmaylov, J. Bloino, G. Zheng, J. L. Sonnenberg, M. Hada, M. Ehara, K. Toyota, R. Fukuda, J. Hasegawa, M. Ishida, T. Nakajima, Y. Honda, O. Kitao, H. Nakai, T. Vreven, J. A. Montgomery, Jr., J. E. Peralta, F. Ogliaro, M. Bearpark, J. J. Heyd, E. Brothers, K. N. Kudin, V. N. Staroverov, R. Kobayashi, J. Normand, K. Raghavachari, A. Rendell, J. C. Burant, S. S. Iyengar, J. Tomasi, M. Cossi, N. Rega, J. M. Millam, M. Klene, J. E. Knox, J. B. Cross, V. Bakken, C. Adamo, J. Jaramillo, R. Gomperts, R. E. Stratmann, O. Yazyev, A. J. Austin, R. Cammi, C. Pomelli, J. W. Ochterski, R. L. Martin, K. Morokuma, V. G. Zakrzewski, G. A. Voth, P. Salvador, J. J. Dannenberg, S. Dapprich, A. D. Daniels, Ö. Farkas, J. B. Foresman, J. V. Ortiz, J. Cioslowski, D. J. Fox, Gaussian 09 Rev. D.01, *Wallingford, CT* (2009).

[17] A. D. Becke, Density-functional exchange-energy approximation with correct asymptotic behavior, *Physical Review A* **38** (1988) 3098-3100. https://doi.org/10.1103/PhysRevA.38.3098

[18] V. Barone, M. Cossi, Quantum Calculation of Molecular Energies and Energy Gradients in Solution by a Conductor Solvent Model, *The Journal of Physical Chemistry A* **102** (1998) 1995-2001. https://doi.org/10.1021/jp9716997

[19] H. Bourzi, R. Oukhrib, B. El Ibrahimi, H. Abou Oualid, Y. Abdellaoui, B. Balkard, S. El Issami, M. Hilali, L. Bazzi, C. Len, Furfural Analogs as Sustainable Corrosion Inhibitors-Predictive Efficiency Using DFT and Monte Carlo Simulations on the Cu(111), Fe(110), Al(111) and Sn(111) Surfaces in Acid Media, *Sustainability* **12(8)** (2020) 3304. https://doi.org/10.3390/su12083304

[20] H. Sun, P. Ren, J. Fried, The COMPASS force field: parameterization and validation for phosphazenes, *Computational and Theoretical Polymer Science* **8** (1998) 229-246. https://doi.org/10.1016/S1089-3156(98)00042-7

[21] E. Echchihbi , R. Salim, M. Ouakki , M. Koudad , L. Guo , M. Azam, N. Benchat, Z. Rais, M. Taleb**,** Corrosion resistance assessment of copper, mild steel, and aluminum alloy 2024-T3 in acidic solution by a novel imidazothiazole derivative, *Materials Today Sustainability* **240** (2023) 100524. https://doi.org/10.1016/j.mtsust.2023.100524

[22] M. Abdallah, Guar Gum as corrosion inhibitor for dissolution of carbon steel in NaCl solution, *Portugaliae Electrochimica Acta* **22** (2004) 161-175. https://doi.org/10.4152/pea.200402161

[23] F. M. Abd El Wahab and A. M. Shams El Din, Effect of Gelatin on the Pitting Corrosion of Iron in Acid and Alkaline Solutions, *British Corrosion Journal* **13(1)** (1978) 39-44. https://doi.org/10.1179/000705978798358716

[24] M. Abdallah, I. Zaafarany, K. S. Khairou, Y. Emad, Natural Oils as Corrosion Inhibitors for Stainless Steel in Sodium Hydroxide Solutions, *Chemistry and Technology of Fuels and Oils* **48(3)** (2012) 234-245. https://doi.org/10.1007/s10553-012-0364-x

[25] M. Abdallah, K. A. Soliman, M. Alfakeer, A. M. Al-bonayan, M. T. Alotaibi, H. Hawsawi, O. A. Hazazi, R. S. Abdel Hameed, M. Sobhi, Mitigation effect of natural Lettuce oil on the corrosion of mild steel in sulfuric acid solution: Chemical, electrochemical, computational aspects, *Green Chemistry Letters and Reviews* **16(1)** (2003) 2249019. https://doi.org/10.1080/17518253.2023.2249019

[26] S. K. Gupta, R. K. Mehta, M. Yadav, O. Dagdag, V. Mehmeti, A. Berisha, E. E. Ebenso, Diazenyl derivatives as efficient corrosion inhibitors for mild steel in HCl medium: Gravimetric, electrochemical and computational approach, *Journal of Molecular Liquids* **382** (2023) 121976. https://doi.org/10.1016/j.molliq.2023.121976

[27] M. R. Albayati, S. Kansız, H. Lgaz, S. Kaya, N. Dege, I. H. Ali, R. Salghi, I. Chung, Synthesis, experimental and theoretical characterization of (E)-2-((2,3-dimethylphenyl)amino)-N'-(furan-2-ylmethylene)benzohydrazide, *Journal of Molecular Structure* **1219** (2020) 128518. https://doi.org/10.1016/j.molstruc.2020.128518

[28] J. Bessone, C. Mayer, K. Jüttner, W. J. Lorenz, AC-impedance measurements on aluminum barrier type oxide films, *Electrochimica Acta* **28** (1983) 171-175. https://doi.org/10.1016/0013-4686(83)85105-6

[29] M. Abdallah, K. A. Soliman, R. Alfattani, A.S. Al-Gorair, A. Fawzy, M. A. A. Ibrahim, Insight of corrosion mitigation performance of SABIC iron in 0.5 M HCl Solutionby tryptophan and histidine: Experimental and computational approaches, *International Journal of Hydrogen Energy* **47(2)** (2022) 12782-12797. https://doi.org/10.1016/j.ijhydene.2022.02.007

[30] S. K. Saha, A. Dutta, P. Ghosh, D. Sukul, P. Banerjee, Adsorption and corrosion inhibition effect of Schiff base molecules on the mild steel surface in 1 M HCl medium: a combined experimental and theoretical approach, *Physical Chemistry Chemical Physics* **17** (2015) 5679-5690. https://doi.org/10.1039/C4CP05614K

[31] T. Gu, B. Tan, J. Liu, J. Chen, H. Wei, F. Zhang, N. Al-Zaqri, W. Li, Insight into the corrosion inhibition performance of Jasmine flower extract on copper in sulfuric acid medium using experimental and theoretical calculation methods, *Journal of Taiwan Institute of Chemical Engineers* **150** (2023) 105047. https://doi.org/10.1016/j.jtice.2023.105047

[32] A.K. Singh, M.A. Quraishi, Inhibiting effects of 5-substituted isatin-based Mannich bases on the corrosion of mild steel in hydrochloric acid solution, *Journal of Applied Chemistry* **40** (2010) 1293-1306. https://doi.org/10.1007/s10800-010-0079-9

[33] M.A. Hegazy, M. Abdallah, M. Alfakeer, H. Ahmed, Corrosion Inhibition Performance of a Novel Cationic Surfactant for protection of Carbon Steel Pipeline in Acidic Media, *International Journal of Electrochemical Science* **13** (2018) 6824-6842. https://doi.org/10.20964/2018.07.53

[34] M. Prajila, A. Joseph, Controlling the Rate of Dissolution of Mild Steel in Sulfuric Acid Through the Adsorption and Inhibition Characteristics of (4-(4-Hydroxybenzylideneamino)-4H-1,2,4-Triazole-3,5-diyl)dimethanol (HATD), *Journal of Bio- and Tribo- Corrosion* **3** (2017) 10. https://doi.org/10.1007/s40735-016-0070-z

[35] M. Abdallah, S. A. Ahmed, H. M. Altass, I. A. Zaafarany, M. Salem, A. I. Aly .E. M. Hussein, Competent inhibitor for the corrosion of zinc in hydrochloric acid based on 2,6-bis-[1-(2-phenylhydrazono)ethyl]pyridine**,** *Chemical Engineering Communications* **206(2)** (2019) 137-148. https://doi.org/10.1080/00986445.2018.1477761

[36] M. Abdallah, T. Al-Habal, R. El-Sayed, M. I. Awad, R. S. Abdel Hameed, Corrosion control of carbon steel in acidic media by nonionic surfactant compounds derived from oxadiazole and

thiadiazol, *International Journal of Electrochemical Science* **17** (2022) 221255. https://doi.org/10.20964/022.12.63

[37] A. Soliz, P. P. Zamora, J. P. Muena, K. Bieger, J. Haribabu, E. Landaeta, A. Arulraj, R. V. Mangalaraja, Experimental and DFT analysis of the concentration dependency of corrosion inhibition by a pyridine Schiff base for mild steel in HCl solution, *Colloids and Surfaces A: Physicochemical and Engineering Aspects* **703** (2024) 135283. https://doi.org/10.1016/j.colsurfa.2024.135283

[38] A. Berisha, F. Podvorica, V. Mehmeti, F. Syla, D. Vataj, Theoretical and experimental studies of the corrosion behavior of some thiazole derivatives toward MS in sulfuric acid media, *Macedonian Journal of Chemistry and Chemical Engineering* **34** (2015) 287-294. https://doi.org/10.20450/mjcce.2015.576

[39] M. A. Amin, K. Khaled, Copper corrosion inhibition in O_2-saturated H_2SO_4 solutions, *Corrosion Science* **52** (2010) 1194-1204. https://doi.org/10.1016/j.corsci.2009.12.035

[40] H. Li, S. Zhang, Y. Qiang, Corrosion retardation effect of a green cauliflower extract on copper in H_2SO_4 solution: Electrochemical and theoretical explorations, *Journal of Molecular Liquids* **321** (2021) 114450. https://doi.org/10.1016/j.molliq.2020.114450

[41] B. Tan, S. Zhang, Y. Qiang, L. Feng, C. Liao, Y. Xu, S. Chen, Investigation of the inhibition effect of Montelukast Sodium on the copper corrosion in 0.5 mol/L H_2SO_4, *Journal of Molecular Liquids* **248** (2017) 902-910.https://doi.org/10.1016/j.molliq.2017.10.111

[42] H. Li, S. Zhang, B. Tan, Y. Qiang, W. Li, S. Chen, L. Guo, Investigation of Losartan Potassium as an eco-friendly corrosion inhibitor for copper in 0.5 M H_2SO_4, *Journal of Molecular Liquids* **305** (2020) 112789. https://doi.org/10.1016/j.molliq.2020.112789

[43] P. Hu, P. Cheng, Y. Wu, L. Guo, A. A. AlObaid, Insight into the corrosion inhibition performance of Capsicum annuum L. leaf extract as corrosion inhibitor for copper in sulfuric acid medium, *Journal of the Taiwan Institute of Chemical Engineers* **161** (2024) 105558. https://doi.org/10.1016/j.jtice.2024.105558